Journal of Inflammation Research

Dovepress
Taylor & Francis Group

Open Access Full Text Article

ORIGINAL RESEARCH

ZnO NPs Attenuate LPS-Induced Inflammation in RAW264.7 Macrophages by Inhibiting NF-κB and JAK1-STAT1/STAT3 Pathways and Reducing ROS

Hui Tang[1,2], Li Zhang[1,2], Chengchen Deng[2,3], Yuechuan Li[2,3], Guiying Ren[2,4], Ziru Sun[2,4], Lebing Chang[2,4], Meihong Xu[2,4], Duanqiang Xiao[2,4], Haijun Zhang[1,2]

[1]Department of Interventional and Vascular Surgery, Shanghai Tenth People's Hospital, School of Medicine, Tongji University, Shanghai, 200072, People's Republic of China; [2]National United Engineering Laboratory for Biomedical Material Modification, Branden Industrial Park, Dezhou, Shandong, 251100, People's Republic of China; [3]Key Laboratory for Biorheological Science and Technology of Ministry of Education, National Local Joint Engineering Laboratory for Vascular Implants, Bioengineering College of Chongqing University, Chongqing, 400044, People's Republic of China; [4]School of Materials Science and Engineering, Shandong University of Technology, Zibo, Shandong, 255000, People's Republic of China

Correspondence: Haijun Zhang, Department of Interventional and Vascular Surgery, Shanghai Tenth People's Hospital, School of Medicine, Tongji University, No. 301, Middle Yanchang Road, Shanghai, 200072, People's Republic of China, Email zhanghaijun@tongji.edu.cn

Background: Macrophage-mediated inflammatory signaling drives pathological inflammation in diverse diseases. Zinc oxide nanoparticles (ZnO NPs) exhibit recognized anti-inflammatory activity, but their precise molecular mechanisms remain unclear. This study investigates the modulatory effects of ZnO NPs on Lipopolysaccharide (LPS)-induced inflammatory and underlying pathways in RAW264.7 macrophages.

Methods: Scanning electron microscopy (SEM) was used to analyze the primary particle sizes of ZnO NPs. Their cytotoxicity on RAW264.7 cells was assessed using the CCK-8 assay. Cells were pretreated with ZnO NPs (0, 0.5, 1, 2, 5 μg/mL) for 1 h, then stimulated with LPS (1 μg/mL) for 24 h. Pro-inflammatory factors (TNF-α, IL-1β, IL-6, iNOS, and COX-2), as well as the anti-inflammatory factor Arg-1, were detected using qRT-PCR, ELISA, or Western blot. RNA-sequencing identified differentially expressed genes (DEGs). Nitric oxide (NO) production, Reactive Oxygen Species (ROS).

Results: ZnO NPs reduced LPS-induced production of NO and pro-inflammatory factors but increased Arg-1 expression. RNA-sequencing identified 2638 DEGs (1822 upregulated, 816 downregulated) between LPS and LPS+ZnO NPs groups. Mechanistically, ZnO NPs exerted anti-inflammatory effects through: (1) blocking NF-κB activation by inhibiting IκB-α degradation and p65 nuclear translocation; (2) suppressing JAK1-mediated STAT1/3 activation and nuclear translocation. They also reduced LPS-induced ROS.

Conclusion: ZnO NPs mitigate LPS-triggered inflammation by targeting NF-κB and JAK1-STAT1/3 pathways, and reducing ROS. These findings provide novel mechanistic insights into the anti-inflammatory effects of ZnO NPs, highlighting their therapeutic potential in macrophage-associated inflammatory disorders.

Keywords: macrophages, ZnO NPs, inflammatory cytokine, NF-κB signaling pathway, JAK-STAT signaling pathway, ROS

Introduction

Inflammation is a crucial biological response, serving as the body's primary defense mechanism against pathogenic invasions, cellular damage, and environmental irritants. Notably, this process exhibits distinct temporal patterns: the transient acute phase promotes tissue repair and the restoration of homeostasis, while sustained chronic inflammation shows strong pathophysiological associations with tumor progression, atherosclerotic cardiovascular diseases, and immune dysregulation syndromes.[1–3] Coordinated by immune cells, vascular systems, and molecular signaling cascades, the inflammatory response triggers precisely regulated cytokine release and chemotactic gradients following cellular injury.[4] This molecular coordination aims to achieve three core biological goals: pathogen elimination, clearance of damaged cells, and tissue structural reconstitution. However, dysregulated or prolonged inflammation can cause

Received: 16 April 2025
Accepted: 26 September 2025
Published: 9 October 2025

persistent tissue damage and evolve into a maladaptive response, which is linked to pathogenesis of metabolic disorders (notably insulin resistance syndromes),[5,6] oncogenic transformation[7] and cardiovascular diseases (CVDs).[8]

Macrophages are pivotal immune cells that orchestrate the entire pathological process, ranging from inflammation to tissue repair, by adopting distinct phenotypes.[9–11] These cells contribute to inflammation by phagocytosing tissue debris and releasing proinflammatory cytokines and proteinases; conversely, they facilitate tissue repair by secreting mediators that promote extracellular matrix (ECM) synthesis, cellular proliferation, and angiogenesis.[11,12] Moreover, macrophages are crucial in mediating the inflammatory response in the progression of CVDs.[13,14] Lipopolysaccharide (LPS), a key proinflammatory stimulus, can activate macrophages to generate large quantities of inflammatory cytokines and mediators, including tumor necrosis factor-alpha (TNF-α), interleukin (IL)-6, IL-1β[15–17] and nitric oxide (NO).[18]

In recent years, nanotechnology has driven significant advancements in scientific innovation. Owing to their ultrasmall size, large specific surface area, unique structural features, and distinct chemical composition, nanomaterials exhibit exceptional properties—making them promising candidates for diverse biomedical applications, such as diagnostics, bioimaging, and drug delivery.[19–23] Zinc oxide nanoparticles (ZnO NPs) have emerged as multifunctional platforms in advanced materials science thanks to their unique physicochemical properties that rendering them highly suitable for various biomedical and biophilic applications.[24] These nanoparticles display excellent chemical stability, high electrochemical coupling efficiency, broad-spectrum light absorption, and outstanding photostability.

Moreover, their large specific surface area, low toxicity, excellent biocompatibility, and biodegradability further underscore their potential for diverse biomedical applications.[25–27] Recent studies have emphasized the multifunctional attributes of ZnO NPs, including antibacterial, antidiabetic, anticancer, wound-healing, and bioimaging capabilities. These properties make ZnO NPs a cost-effective and biocompatible alternative for a wide range of biomedical applications.[24,28–31] Furthermore, ZnO NPs have proven effective in alleviating polymer-wear-particle-induced inflammatory osteolysis, underscoring their therapeutic potential in inflammatory and degenerative bone disorders.[32] In a notable study by Nagajyothi et al, demonstrated that ZnO NPs exert moderate antioxidant activity and anti-inflammatory effects, further supporting their potential as therapeutic agents.[33] Additionally, ZnO NPs have exhibited anti-inflammatory effects and protective properties in chondrocytes under hypoxic conditions.[34,35] However, the precise mechanisms underlying these anti-inflammatory actions, particularly in macrophages, remain largely unexplored.

Thus, this study aims to evaluate the anti-inflammatory effects of ZnO NPs in RAW264.7 macrophages and elucidate the underlying molecular mechanisms, thereby exploring their broader therapeutic potential for macrophage-associated inflammatory disorders.

Materials and Methods

Cell Culture

The RAW264.7 murine macrophage cell line was obtained from the Cell Bank of the Chinese Academy of Sciences (Shanghai, China). Cells were cultured in high-glucose Dulbecco's Modified Eagle Medium (DMEM) supplemented with 10% fetal bovine serum (FBS), 100 U/mL penicillin, and 100 μg/mL streptomycin. The cells were maintained in a humidified incubator at 37 °C with 5% carbon dioxide (CO_2) atmosphere.

Characterization of ZnO NPs

Zinc oxide nanoparticles (ZnO NPs; Z820746) were purchased from Macklin Biochemical Co., Ltd. (Shanghai, China). The morphological characteristics of ZnO NPs were analyzed using a scanning electron microscope (SEM, Apreo 2C, Thermo Scientific, MS, USA) at an accelerating voltage of 5 kV with secondary electron detection, which revealed a spherical morphology. More than 400 particles were measured to calculate the mean size and characterize the distribution of distinct particle sizes.

Reagents and Antibodies

Lipopolysaccharides (LPS; L8880) derived from *Escherichia coli* O111:B4 were obtained from Solarbio Life Science (Beijing, China). Ruxolitinib (HY-50856), Lyso Green kit (HY-KD1027), and JC-1 kit (HY-K0601) were purchased from

MedChemExpress (MCE, NJ, USA). Cell Counting Kit-8 (CCK-8; PF00004) was purchased from Proteintech Biological Technology Co., Ltd., (Wuhan, China). Enzyme-Linked Immunosorbent Assay (ELISA) kit for TNF-α (EK0527), IL-1β (EK0394), and IL-6 (EK0411) were purchased from BOSTER Biological Technology Co., Ltd., (Wuhan, China). DCFH-DA (KGA7308) was obtained from KeyGEN BioTECH (Nanjing, China). Total NO Assay Kit (S0021S), Endotoxin detection reagents kit (C0273S) and Nuclear/Cytoplasmic Isolation Kit (P0028) were purchased from Beyotime Biotechnology Co., Ltd. (Shanghai, China).

Antibodies against phospho-p38 (Thr180/Thr182; #4511) and phospho-JAK1(Tyr1034/1035; #74129S) were purchased from Cell Signaling Technology (Beverly, MA, USA). JAK1 (R382163), JAK2 (R24775), Phospho-STAT3 (Tyr705; R381552), STAT1 (R25799), and phospho-PI3K p85/p55 (Tyr467/Tyr199; #310164) were obtained from ZEN-BIOSCIENCE (Chengdu, China). Phospho-JAK2 (Y1007+Y1008; T56570S), phospho-STAT1 (Tyr701; TP56498S), phospho-Akt (Ser473; T40067S), NOD1 (P42567-1S) and NOD2 (PC7084S) were purchased from Abmart (Shanghai, China). STAT3 (10253-2-AP), and NF-κB p65 (10745-1-AP) were purchased from Proteintech Biological Technology Company (Wuhan, China). COX2 (ab179800), iNOS (ab178945), Arginase 1 (Arg-1; ab124917), IκB-α (ab32518), p38 (ab170099), PI3K p85alpha (ab191606), AKT1+AKT2+AKT3 (ab179463), phospho-JNK (T183+T183+T221; ab124956), JNK (ab179461), phospho-ERK1 (T202 + Y204) + ERK2 (T185 +Y187; ab278538) and ERK (ab184699) were obtained from Abcam Biotech (Cambridge, MA, USA).

CCK-8 Assay

Briefly, RAW264.7 cells were seeded in 96-well culture plates at a density of 1×10^4 cells per well and cultured overnight. The cells were then treated with ZnO NPs at different concentrations (1, 5, 10, 20, 50 μg/mL) or normal medium (control group) for 24 h. After the treatment, 10 μL of CCK-8 reagent was added to each well, followed by incubation for 1 h. Absorbance was measured at 450 nm using a microplate reader (BioTek ELX800, VT, USA). Cell viability was calculated as the percentage of absorbance for each ZnO NPs-treated group relative to the control.

ZnO NPs Endotoxin Detection

To determine whether ZnO NPs were contaminated with endotoxins, we performed the detection using an endotoxin detection kit. The detailed procedures, with strict contamination control measures, are as follows: prepare sterile, endotoxin-free centrifuge tubes, ensure all pipette tips, pipettes, and containers used are endotoxin-free to avoid exogenous contamination. Add 20 μL of endotoxin-free water (detection-grade, as blank control), endotoxin standard solution at concentrations of 0.010, 0.025, 0.050, 0.075, and 0.100 EU/mL (for standard curve calibration) or ZnO NPs sample to be tested to each pre-prepared tube, respectively. Add 10 μL of endotoxin detection reagent working solution to each tube, incubate at 37 °C in the dark for 25 min. After the first incubation, add 20 μL of chromogenic reagent solution to each tube, continue incubating the tubes at 37 °C in the dark for 6 min. Add 40 μL of chromogenic stop solution to each tube immediately after the second incubation. Measure the absorbance of each tube at a wavelength of 405 nm using a microplate reader (BioTek ELX800). Endotoxin concentrations in the ZnO NPs sample were calculated based on the standard curve.

Quantitative Real-Time Polymerase Chain Reaction (qRT-PCR) Assay

Cells (1×10^5 cells/well) were seeded in 12-well culture plates and subjected to pretreatment with ZnO NPs (0, 0.5, 1, 2, and 5 μg/mL) for 1 h, followed by stimulation with LPS (1 μg/mL) for 24 h. Total RNA was isolated using the Trizol™ reagent-based extraction method (TaKaRa Biotech, Dalian, China). Subsequently, complementary DNA (cDNA) was synthesized from 1 μg of RNA templates using PrimeScript™ RT Master Mix (TaKaRa Biotech).

For quantitative amplification, reactions were performed on a SLAN-96S thermal cycler (Hongshi Instruments, Shanghai, China) using SYBR® Green-based fluorescence detection. Custom-designed primer pairs (detailed in Table 1) were used for targeted transcript quantification under optimized thermocycling conditions: an initial denaturation step at 95 °C for 30 s (1 cycle); followed by 40 amplification cycles, each consisting of denaturation at 94 °C for 5 s and primer-template annealing at 60 °C for 34 s.

Table 1 Primers Used in qRT-PCR Study

Target gene	Forward Primer Sequence (5'-3')	Reverse Primer Sequence (5'-3')
iNOS	GACGAGACGGATAGGCAGAGATTG	AACTCTTCAAGCACCTCCAGGAAC
COX-2	TGGTGCCTGGTCTGATGATGTATG	GTCTGCTGGTTTGGAATAGTTGCTC
IL-1β	TCGCAGCAGCACATCAACAAG	TCCACGGGAAAGACACAGGTAG
IL-6	CTCCCAACAGACCTGTCTATAC	CCATTGCACAACTCTTTTCTCA
TNF-α	ACCCTCACACTCACAAACCAC	TCTTTGAGATCCATGCCGTTGG
GAPDH	ACTCCACTCACGGCAAATTCAAC	ACACCAGTAGACTCCACGACATAC

Target mRNA expression levels were normalized to the housekeeping gene glyceraldehyde-3-phosphate dehydrogenase (GAPDH) for quantitative calibration, and relative expression was calculated using the comparative threshold cycle ($2^{-\Delta\Delta Ct}$) algorithm.[36] To ensure experimental rigor, all assays were performed with three biological replicates, and mean values were used for statistical analysis.

Western Blotting Assay

Total protein lysates were prepared using RIPA Lysis Buffer™ (Beyotime). For subcellular fractionation, a Nuclear/Cytoplasmic Isolation Kit (Beyotime) was used, following differential centrifugation techniques. Protein quantification was quantified via bicinchoninic acid (BCA) assay to ensure standardized loading (30 μg per lane) onto 8% or 10% sodium dodecyl sulfate-polyacrylamide gel electrophoresis (SDS-PAGE), followed by transfer to a polyvinylidene difluoride (PVDF) membrane (Millipore, Billerica, MA, USA). After transfer, membranes were blocked in in 5% skim milk for 2 h at room temperature, then subjected to sequential immunodetection: membranes were incubated with primary antibodies overnight at 4 °C, followed by incubation with secondary antibodies for 1 h. Between each step, membranes were washed three times with Tris-buffered saline with Tween 20 (TBST), with each wash lasting 5 min. GAPDH (1:10,000 dilution) and β-actin (1:20,000 dilution) were used as housekeeping proteins, while LaminB1 (1:2000 dilution) served as the internal reference for nuclear proteins. Protein signals were visualized using a Chemiluminescence Imaging System (ShenHua Bio, Hangzhou, China). Densitometric analysis of immunoreactive bands was performed using ImageJ software, with data derived from three technical replicates.

JC-1-Based Mitochondrial Membrane Potential ($\Delta\psi_m$) Detection Assay

To assess changes in mitochondrial membrane potential ($\Delta\psi_m$) of RAW264.7 cells, the JC-1 Mitochondrial Membrane Potential Assay Kit was used. Briefly, RAW264.7 cells were seeded in 12-well plates at a density of 1×10^5 cells/well and cultured overnight. Subsequently, the cells were treated with ZnO NPs at a concentration of 5 μg/mL for 24 h. After treatment, the cells were washed three times with PBS, then stained with 2 μM JC-1 working solution for 15 min at 37°C in the dark. Following staining, the cells were washed three times with PBS, and fluorescent images were acquired at 200× magnification using a fluorescence microscope (OPTIKA, Ponteranica, Italy). Both red fluorescence (emitted by JC-1 aggregates, indicative of high $\Delta\psi_m$) and green fluorescence (emitted by JC-1 monomers, indicative of reduced $\Delta\psi_m$) were captured using the appropriate excitation/emission filter sets. Cellular fluorescence intensity was quantified using ImageJ software.

Acridine Orange (AO) Hydrochloride Assay for Lysosomal Integrity Evaluation

To assess lysosomal integrity in RAW264.7 cells, the AO staining assay was performed. RAW264.7 cells were seeded in 12-well plates at a density of 1×10^5 cells/well and cultured overnight. Cells were then treated with 5 μg/mL ZnO NPs for 24 h. After treatment, the cells were washed with PBS and incubated with 1 μM AO for 20 min at 37 °C in the dark. Following three additional washes with PBS to remove unbound dye, fluorescent images were captured at 400× magnification using a fluorescence microscope (OPTIKA). Fluorescence intensity (red emission indicating healthy lysosomes; green emission indicating lysosomal damage) was quantified using ImageJ software.

Immunofluorescence Assay

For cellular immunofluorescence staining, cells were washed three times with PBS (5 min/cycle). They were then fixed with 4% paraformaldehyde (PFA) for 20 min, followed by three additional PBS washes. Fixed cells were permeabilized with 0.5% Triton X-100 for 20 min. After another PBS wash and blocking with 3% bovine serum albumin (BSA) in PBS for 30 min at room temperature, the cells were co-incubated overnight at 4 °C with primary antibodies against iNOS (1:300 dilution) and Arg-1 (66129-1-Ig, 1:300 dilution; Proteintech). Following three PBS washes, cells were co-incubated with CoraLite594-conjugated goat anti-mouse (1:400 dilution) and CoraLite488-conjugated goat anti-rabbit (1:400 dilution) secondary antibodies for 1 h at room temperature in the dark. Nuclei were counterstained with 4',6-diamidino-2-phenylindole (DAPI) for 3 min in the dark. Fluorescent images were acquired at 400× magnification using a fluorescence microscope (OPTIKA). The analysis of immunofluorescence was quantified by using the Image J software.

Confocal Laser Microscopy Analysis

RAW264.7 cells were seeded in small confocal laser dishes at a density of 1×10^3 cells/well. The cells were pretreated with ZnO NPs at concentrations of 0, 0.5, 1, 2, and 5 μg/mL for 1 h, followed by stimulation with LPS for 24 h. After the above treatments, the cells were washed with PBS, fixed with 4% PFA for 20 min, permeabilized with 0.5% Triton X-100 for 20 min, and blocked with 3% BSA in PBS for 30 min. Subsequently, the cells were incubated with primary antibodies against STAT1 (10144-2-AP, 1:300 dilution; Proteintech) and STAT3 (1:300 dilution) separately at 4 °C overnight. After three washes with PBS, cells were incubated with CoraLite488-conjugated goat anti-rabbit secondary antibody (1:400 dilution) for 1 h at room temperature in the dark. Finally, cells were stained with DAPI for 3 min in the dark. Fluorescent images were acquired using an Olympus FV3000 confocal laser scanning microscope (Olympus, Tokyo, Japan) at 600× magnification.

Reactive Oxygen Species (ROS) Detection

Oxidative stress was quantified using the cell-permeable fluorescent probe DCFH-DA following an esterase-dependent activation protocol. Briefly, cellular suspensions were incubated with 10 μM DCFH-DA at 37 °C for 30 min, followed by three washes with PBS to remove de-esterified fluorophores. Fluorescence signals were acquired using a flow cytometer (Beckman Coulter, CA, USA) equipped with a 488 nm argon laser for excitation and a 525 nm bandpass filter for emission. Statistical analysis of ROS production was performed using data from three independent experimental replicates to determine significance.

Cytokine Secretion Profiling via ELISA

Following LPS stimulation, cell supernatants were collected for quantification of TNF-α, IL-1β, and IL-6 levels using ELISA kits. Briefly, 100 μL of the diluted sample was added in pre-coated microwells at 37 °C for 90 min. Negative and positive controls were included, and each test was performed in duplicate. The assay was conducted as follows: sequential incubation with biotinylated detection antibodies at 37 °C for 1 h; subsequent five-cycle washing with 300 μL of buffer per well; addition of 100 μL of enzyme conjugate and incubation at 37 °C for 30 min; five additional washes; addition of 90 μL of horseradish peroxidase substrate solution and incubation at 37 °C in the dark for 15 min; and finally, addition of stop solution. Optical density was measured at 450 nm using a BioTek (ELX800) microplate reader. Data were normalized against calibration standards via four-parameter logistic regression, and sample concentrations were calculated using the standard curve as described previously.[37]

Nitric Oxide (NO) Quantification

Cell culture supernatants were collected to analyze NO metabolite analysis using a Total NO Assay Kit, following the manufacturer's protocol. Absorbance was measured at 540 nm using a microplate reader (ELX800). The experiment was performed in three independent biological replicates.

High-Throughput Transcriptomic Profiling and Functional Annotation

For RAW264.7 macrophages in three experimental groups (Control, LPS-challenged, and LPS+ ZnO NPs co-treated), three independent biological replicates per group were subjected to rigorous RNA integrity validation prior to the

preparation of strand-specific cDNA libraries. High-depth sequencing was performed on the Illumina NovaSeq 6000 platform (Novogene Co., Ltd., Shanghai, China). Transcripts with $|\log_2\text{Fold Change}| \geq 1$and padj < 0.05 were defined as differentially expressed genes (DEGs). Gene Ontology (GO) and Kyoto Encyclopedia of Genes and Genomes (KEGG) pathway enrichment analyses of DEGs were conducted using the Cluster Profiler package.[38]

Statistical Analysis

Data are expressed as means ± standard deviation (SD). All experiments were performed in triplicate ($n \geq 3$). For statistical analysis, Student's *t* test was used to compare differences between two groups, while one-way analysis of variance (ANOVA) was applied for comparisons involving more than two groups. All statistical computations were performed using GraphPad Prism 8.0 (GraphPad, Inc., La Jolla, CA, USA). A P value < 0.05 was considered statistically significant.

Results

The Effects of ZnO NPs on RAW264.7 Macrophages Activity

The primary particle size and morphology of ZnO NPs were characterized using SEM. SEM micrographs (Figure 1A and B) revealed that the ZnO NPs exhibited a distinct prismatic morphology, characterized by well-defined angular edges and a uniform structural profile. To quantify primary particle size distribution, 400 individuals ZnO NPs were randomly selected from three independent SEM fields (50,000× magnification) to ensure statistical representativeness. As shown in Figure 1C, the ZnO NPs exhibited a broad but well-characterized size range of 55.19–620.5 nm, with an average diameter of 180.7 ± 84.77 nm and a median diameter of 159.0 nm. The 100–150 nm size class was the most abundant, accounting for 32% of total particles; this was followed by the 150–200 nm class (23%) and the 200–250 nm class (~15%) and the 50–100 nm class (~12%). Notably, particles within the 50–250 nm range collectively constituted 82.0% of all measured NPs, confirming that the majority of ZnO NPs fall within a biologically relevant size range for macrophage interactions.

To assess the cytotoxicity of ZnO NPs on RAW264.7 cells, cell viability was determined by the CCK-8 assay. RAW264.7 cells were treated with various concentrations of ZnO NPs (1, 5 10, 20 and 50 μg/mL) for 24 h. As shown in Figure 1D, ZnO NPs exhibited no significant cytotoxicity at low concentrations (≤5 μg/mL). We further investigated whether 5 μg/mL of ZnO NPs affects cellular mitochondrial membrane potential and lysosomal membrane integrity. Results revealed that 5 μg/mL ZnO NPs had no impact on mitochondrial membrane potential or Lysosomal integrity compared with the control group (Supplementary Figure 1A and B). To further confirm whether 5 μg/mL ZnO NPs were contaminated with endotoxins, we used a standard endotoxin detection kit to quantify the endotoxin content in the 5 μg/mL ZnO NPs sample. The results showed that the endotoxin concentration in this sample was below the kit's lower limit of detection (0.010 EU/mL), as shown in Supplementary Figure 1C and D. This finding confirms that the 5 μg/mL ZnO NPs used in our experiments were free of endotoxin contamination, supporting their safe use in our subsequent in vitro inflammation assays. Collectively, these results demonstrated that 5 μg/mL ZnO NPs did not affect cell viability, nor did they trigger mitochondrial membrane potential dysfunction or lysosomal integrity impairment and are free of endotoxin contamination. Therefore, ZnO NPs at concentrations of 0.5, 1, 2, and 5 μg/mL were selected for subsequent experiments.

To identify the optimal LPS concentration for inducing the expression of inflammatory factors (TNF-α, IL-1β, and IL-6), RAW264.7 cells were treated with LPS at 10 ng/mL, 100 ng/mL, or 1000 ng/mL (ie, 1 μg/mL) for 24 h. As shown in Supplementary Figure 2A, only LPS at a concentration of 1000 ng/mL significantly increased TNF-α mRNA levels compared to the control group. In contrast, LPS at both 100 ng/mL and 1000 ng/mL significantly upregulated the mRNA expression of IL-1β and IL-6 (Supplementary Figure 2B and C). Notably, LPS at 10 ng/mL had no effect on the mRNA expression of TNF-α, IL-1β, or IL-6. Therefore, 1μg/mL LPS was selected as the induction concentration for subsequent experiments.

Bright-field microscopy images demonstrated that RAW264.7 cells treated with 1 μg/mL LPS for 24 h displayed distinct morphological alterations compared to untreated control cells: specifically, increased cell volume, extended pseudopodia, and a clear shape transition from round to oval or fusiform (Figure 1E). Additionally, when cells were co-incubated with 1 μg/mL LPS and ZnO NPs at different concentrations (0.5, 1, 2, and 5 μg/mL) for 24 h, the CCK-8 assay

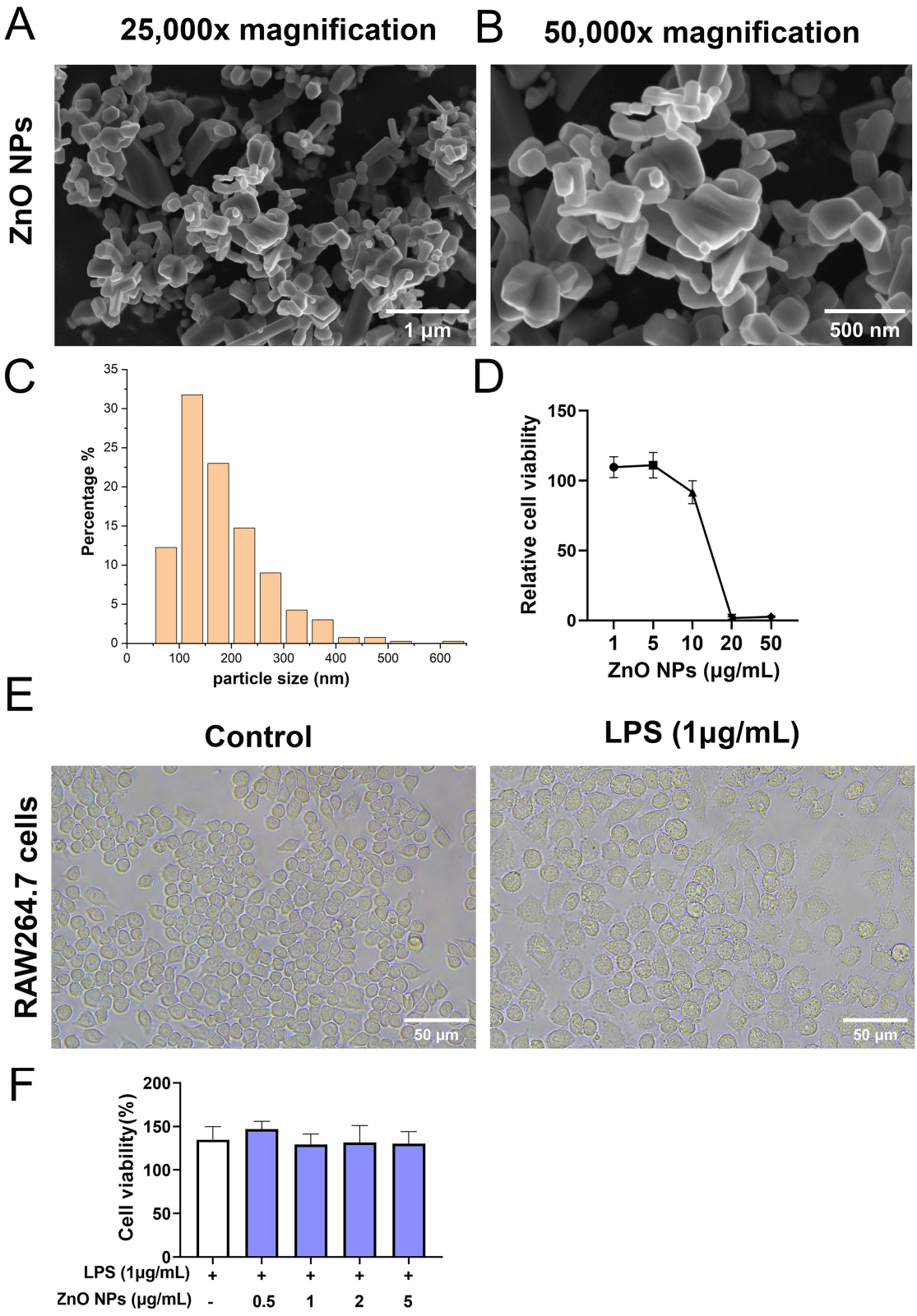

Figure 1 Cell viability of RAW264.7 macrophages treated with ZnO NPs. (**A** and **B**) Representative SEM images illustrating the morphology and size of ZnO NPs. (**C**) Quantitative analysis of the size distribution of ZnO NPs. (**D**) RAW264.7 cells were treated with ZnO NPs (1–50 μg/mL) for 24 h; cell viability was assessed using the CCK-8 assay. (**E**) Morphological observation of RAW264.7 cells in the control and LPS-treated groups via light microscopy (400× magnification). (**F**) RAW264.7 cells were pretreated with ZnO NPs (0, 0.5, 1, 2, and 5 μg/mL) for 1 h, then treated with LPS (1 μg/mL) for 24 h; cell viability was assessed using the CCK-8 assay.

https://doi.org/10.2147/JIR.S534720

revealed no cytotoxicity (Figure 1F). Collectively, these results confirm two key points: (1) 1 μg/mL LPS effectively induces activation-associated morphological changes in RAW264.7 cells; (2) the tested concentrations of ZnO NPs (0.5–5 μg/mL) do not elicit cytotoxic effects when combined with 1 μg/mL LPS, confirming their suitability for subsequent investigations into anti-inflammatory mechanisms.

ZnO NPs Attenuate LPS-Induced NO Production and the Expression of Pro-Inflammatory Cytokines in RAW264.7 Cells

It is well-documented that NO contributes to the regulate of inflammation, while pro-inflammatory cytokines drive its progression. To assess the anti-inflammatory effects of ZnO NPs in LPS-stimulated RAW264.7 cells, the cells were pretreated with different concentrations of ZnO (0, 0.5, 1, 2, and 5 μg/mL) for 1h, followed by co-stimulation LPS (1 μg/mL) for 24 h. The results indicated that ZnO NPs significantly reduced LPS-induced NO production at concentrations of 2 and 5 μg/mL (Figure 2A). Additionally, ZnO NPs significantly reduced both the mRNA and protein levels of TNF-α, IL-1β, and IL-6 in a concentration-dependent manner (Figure 2B–G). These findings demonstrate that ZnO NPs effectively suppress LPS-induced NO release and pro-inflammatory responses, thereby highlighting their anti-inflammatory properties in macrophage-mediated inflammation.

ZnO NPs Suppress M1 Polarization and Enhance M2 Polarization in RAW264.7 Macrophages

To evaluate the effect of ZnO NPs on the polarization of RAW264.7 macrophages from the M1 to the M2 polarization, the following experiments were performed. As widely recognized, the expression of iNOS (a canonical M1 macrophage marker) and COX-2 are key indicators of the oxidative-inflammatory state in cells.[39] Using the same induction protocol described above, we evaluated the impact of ZnO NPs on LPS-induced expression of iNOS, COX-2, and Arg-1 (a canonical M2 marker).

As depicted in Figure 3A and B, ZnO NPs significantly suppressed LPS-induced upregulation of iNOS and COX-2 mRNA levels in a concentration-dependent manner. At the protein level, 5 μg/mL ZnO NPs markedly inhibited the LPS-induced elevation of iNOS protein levels, while COX-2 expression was significantly reduced in the presence of 2 and 5 μg/mL ZnO NPs (Figure 3C). In contrast, ZnO NPs at 5 μg/mL significantly upregulated Arg-1expression (Figure 3D).

Furthermore, we performed immunofluorescence co-staining to detect the expression of iNOS and Arg-1. As shown in Figure 3E, LPS treatment significantly upregulated iNOS protein expression while markedly downregulating Arg-1 protein expression. In contrast, 5 μg/mL ZnO NPs significantly upregulated Arg-1 protein expression and downregulated iNOS protein expression. The results of immunofluorescence staining were in line with those from Western blot analysis (Figure 3F). Collectively, these findings demonstrate that the tested higher concentrations of ZnO NPs—particularly 5 μg/mL—suppress M1 macrophage polarization and promote M2 polarization.

Identification of Inflammatory Signaling Pathways Modulated by ZnO NPs in LPS-Stimulated RAW264.7 Cells via High-Throughput Approaches

To further explore the anti-inflammatory mechanisms of ZnO NPs, we performed transcriptomic analysis on three groups of RAW264.7 cells: untreated control, LPS-stimulated, and LPS + ZnO NPs (5 μg/mL) co-treated. The heatmap illustrates gene expression profiles across the three groups, revealing that ZnO NPs exert distinct modulatory effects on the LPS-induced transcriptional changes in treated cells (Figure 4A).

A total of 3118 differentially expressed genes (DEGs) were identified between the control and LPS groups ($|\log_2\text{FoldChange}| \geq 1.0$, padj < 0.05), of which 2068 were upregulated and 1050 were downregulated in the LPS-induced group relative to the control. Additionally, 2638 DEGs were identified between the LPS and LPS+ZnO NPs groups ($|\log_2\text{FoldChange}| \geq 1.0$, padj < 0.05), with 1822 upregulated and 816 downregulated in the LPS+ZnO NPs group relative to the LPS group.

The Venn diagram revealed that 829 DEGs were shared between the "LPS vs Control" and "LPS+ZnO NPs vs LPS" comparisons, while 2289 DEGs were unique to the "LPS vs Control" group and 1809 DEGs were specific to the "LPS +ZnO NPs vs LPS" group (Figure 4B). To further prioritize functionally relevant transcriptional changes, we selected the

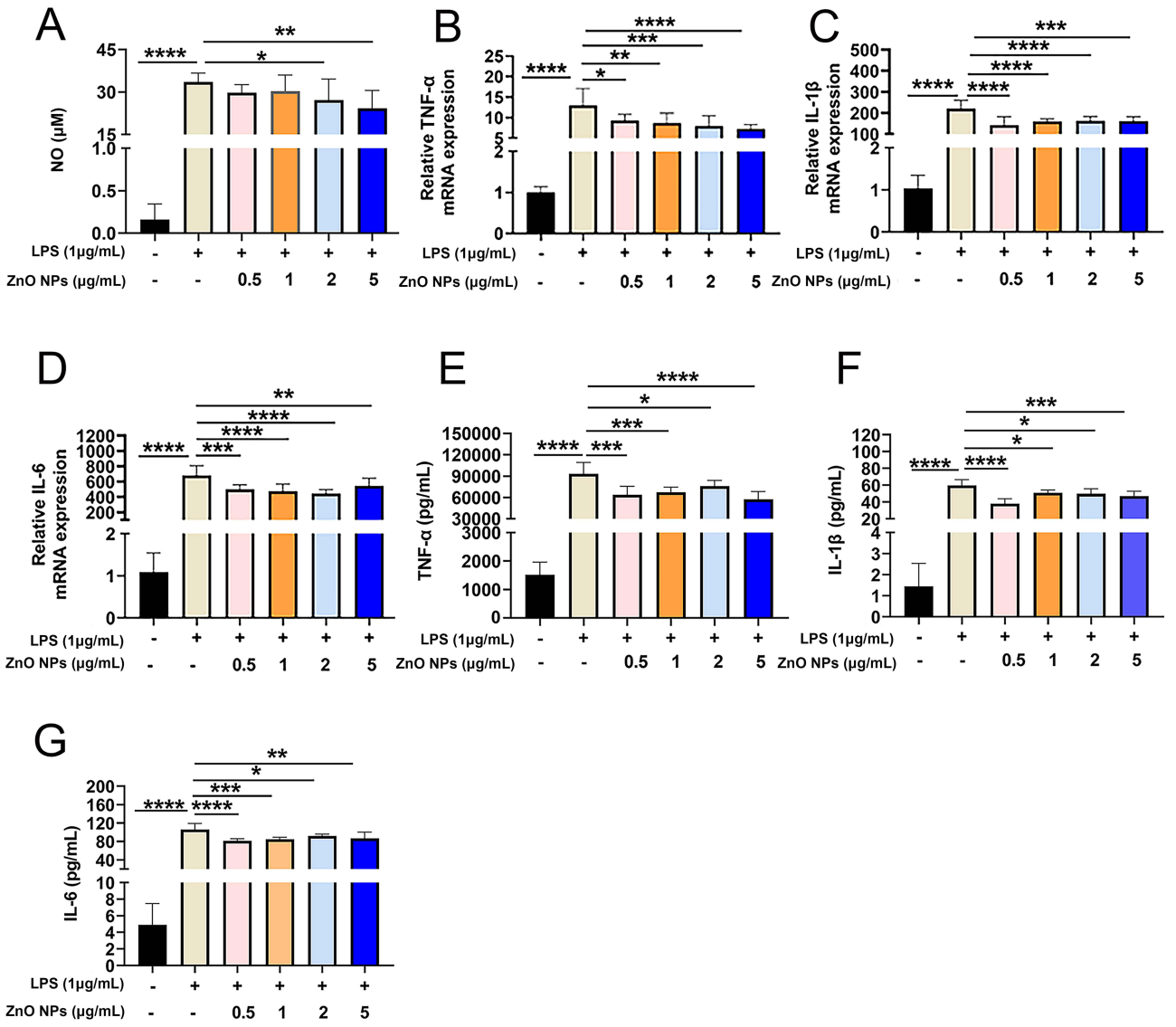

Figure 2 ZnO NPs inhibit LPS-induced NO production and pro-inflammatory cytokine expression in RAW264.7 cells. RAW264.7 cells were pretreated with ZnO NPs (0–5 μg/mL) for 1 h prior to stimulation with LPS (1 μg/mL) for 24 h. (**A**) NO production was detected. (**B**–**G**) The levels of TNF-α, IL-1β, and IL-6 were analyzed by qPCR and ELISA. Data are presented as mean ± SD and analyzed using one-way ANOVA. *p < 0.05, **p < 0.01, ***p < 0.001 and ****p < 0.0001.

top 10 most significantly upregulated and downregulated DEGs for each comparison group. Detailed information for these genes is provided in Supplementary Table 1.

Additionally, KEGG pathway enrichment analysis of upregulated DEGs revealed the top 30 enriched signaling pathways, many of which are inflammation-related—including the TNF-α signaling pathway, Janus kinase-signal transducer and activator of transcription (JAK-STAT) signaling pathway, nuclear factor kappa B (NF-κB) signaling pathway, nucleotide-binding oligomerization domain (NOD)-like receptor signaling pathway, phosphatidylinositol 3-kinase-protein kinase B (PI3K/Akt) pathway, and mitogen-activated protein kinase (MAPK) pathway—all of which are activated by LPS (Figure 4C and Supplementary Table 2). In contrast, KEGG analysis of downregulated DEGs following ZnO NPs treatment identified pathways related to cell cycle regulation, DNA replication, and the Fanconi anemia pathway (Figure 4D).

For GO enrichment analysis, upregulated DEGs were enriched in biological processes (BP) such as the inflammatory response, cellular components (CC) including the external side of the plasma membrane, and molecular functions (MF) like cytokine activity (Figure 4E). Conversely, downregulated DEGs following ZnO NPs treatment were enriched in GO

https://doi.org/10.2147/JIR.S534720

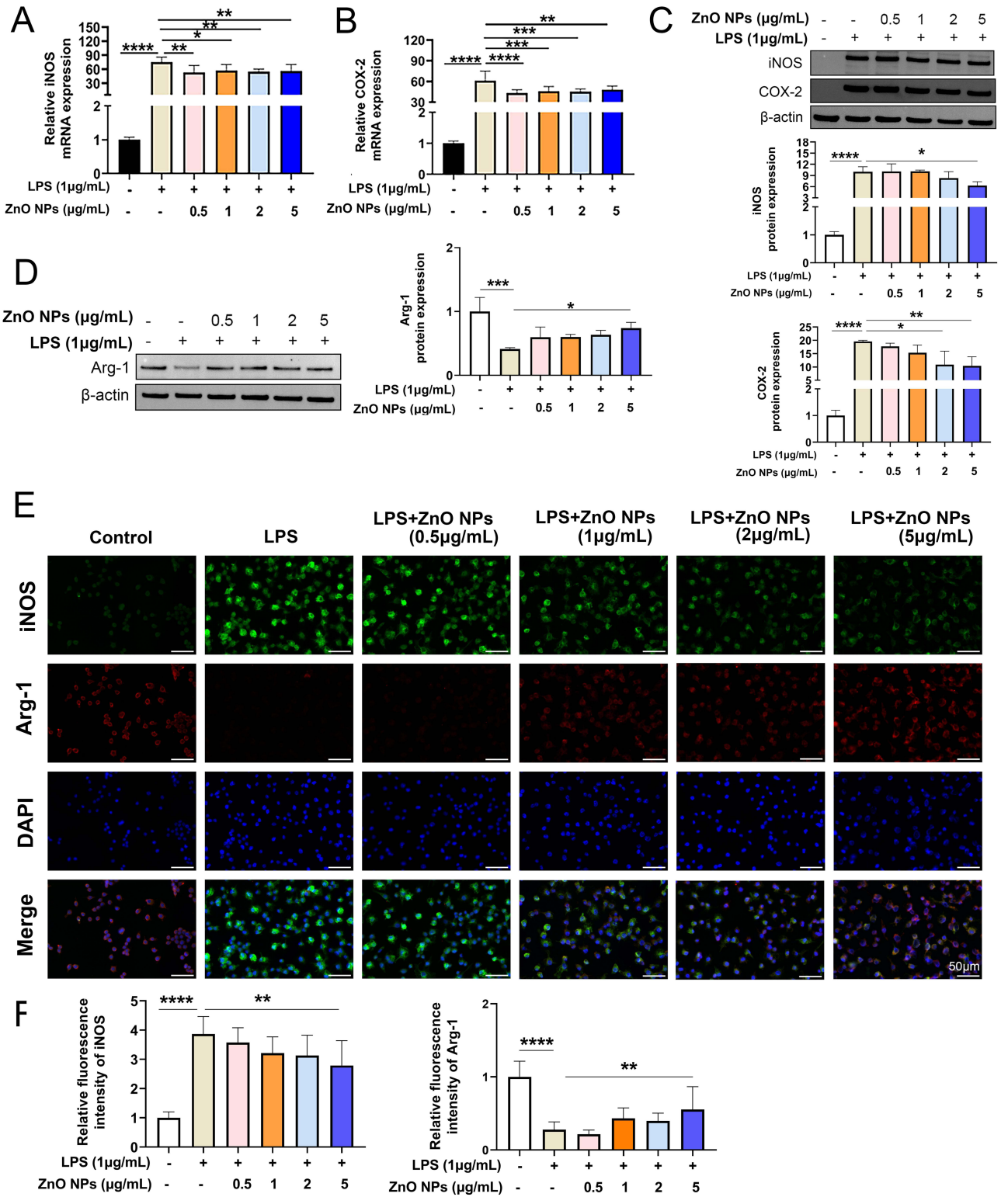

Figure 3 ZnO NPs inhibit LPS-induced iNOS and COX-2 expression and increase Arg-1 expression in RAW264.7 cells. RAW264.7 cells were pretreated with ZnO NPs (0–5 μg/mL) for 1 h, followed by co-stimulation with LPS (1 μg/mL) for 24 h. (**A**–**C**) The mRNA and protein expression levels of iNOS and COX-2 were analyzed by qPCR and Western blot. (**D**) The protein expression of Arg-1 was analyzed by Western blot. (**E** and **F**) Fluorescence intensities of the iNOS and Arg-1 were detected by cell immunofluorescence staining. Data are presented as mean ± SD and were analyzed using one-way ANOVA. *p<0.05, **p < 0.01, ***p<0.001 and ****p<0.0001.

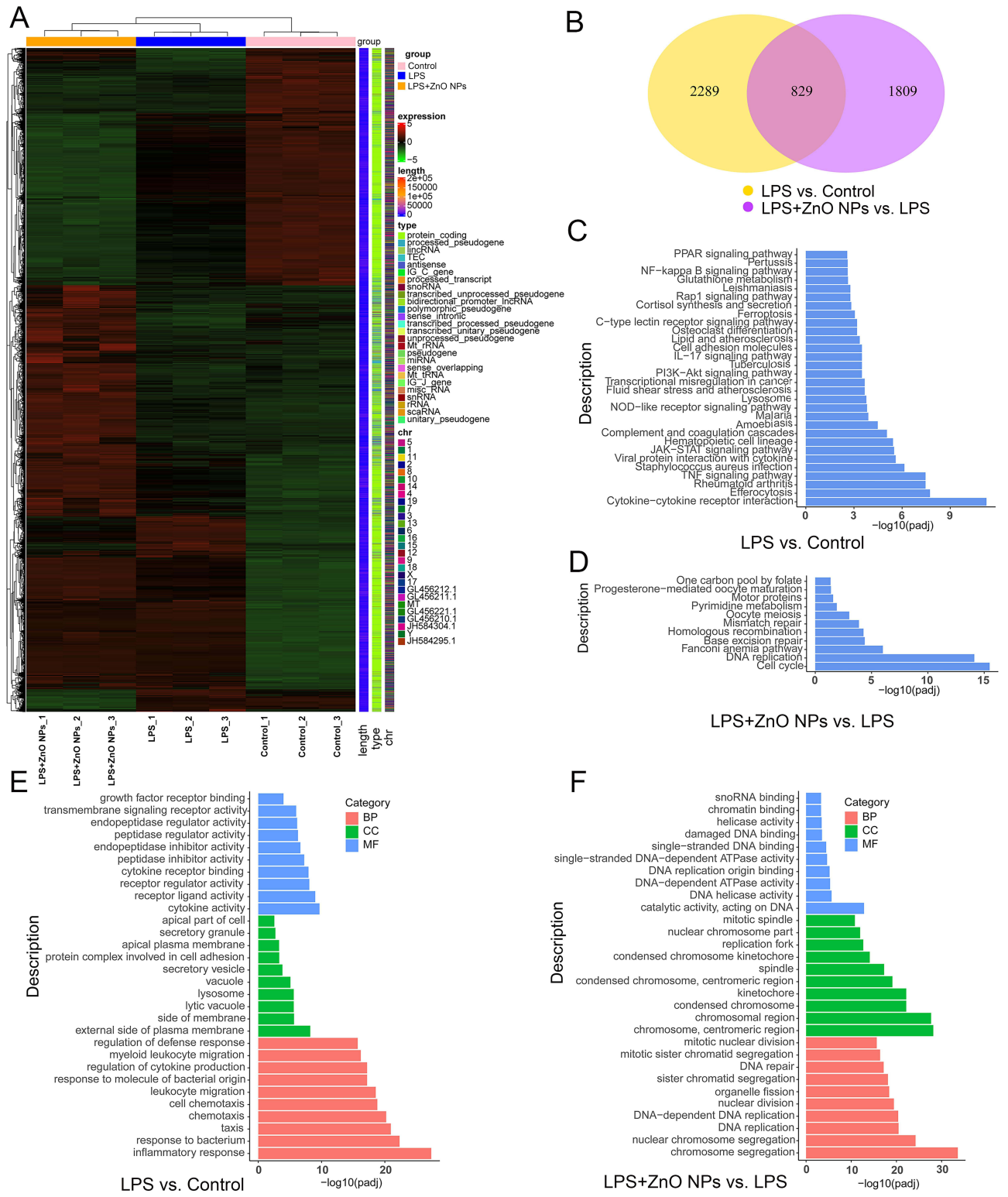

Figure 4 Transcriptomic analysis reveals that ZnO NPs alleviate LPS-induced inflammatory dysregulation in RAW264.7 cells. (**A**) Representative heatmap of DEGs identified via transcriptomic analysis. (**B**) Venn diagram showing the number of DEGs in "LPS vs Control" and "LPS+ZnO NPs vs LPS" comparisons. KEGG pathway enrichment analysis: (**C**) for upregulated DEGs in the "LPS vs Control" comparisons, and (**D**) for downregulated DEGs in the "LPS+ZnO NPs vs LPS" comparisons. GO enrichment analysis: (**E**) for upregulated DEGs in the in "LPS vs Control" comparisons and (**F**) downregulated genes in "LPS+ZnO NPs vs LPS" comparisons. The KEGG pathways and GO terms were ranked by -Log_{10} of the enrichment adjusted p-value.

https://doi.org/10.2147/JIR.S534720

terms including chromosome segregation (BP), chromosome centromeric region (CC), and catalytic activity acting on DNA (MF) (Figure 4F).

ZnO NPs Inhibit LPS-Induced Activation of the IκB-α/NF-κB Signaling Pathway in RAW264.7 Macrophages

KEGG pathway enrichment analysis revealed that the NF-κB pathway mediates LPS-induced inflammatory responses in RAW264.7 cells. To further investigate whether ZnO NPs inhibit LPS-induced NF-κB activation, changes in IκB-α and NF-κB p65 protein levels were evaluated via Western blot analysis. As shown in Figure 5A and B, ZnO NPs effectively suppressed LPS-induced IκB-α degradation and the nuclear translocation of cytoplasmic NF-κB p65, in a concentration-dependent manner. These results demonstrate that ZnO NPs alleviate LPS-induced inflammatory responses in RAW264.7 cells by inhibiting the IκB-α/NF-κB signaling pathway.

ZnO NPs Inhibit LPS-Induced Activation of the JAK1-STAT1/STAT3 Signaling Pathway in RAW264.7 Macrophages

Consistent with KEGG pathway enrichment analysis, the JAK/STAT signaling pathway was also activated by LPS. As is well established, STAT1 and STAT3—key transcription factors in the JAK/STAT pathway—play critical roles in LPS-induced inflammatory responses. To explore whether ZnO NPs regulate STAT signaling under LPS stimulation, the same induction protocol described above was used. As shown in Figure 6A, only 5 μg/mL ZnO NPs significantly inhibited LPS-induced phosphorylation of STAT1 and STAT3 (p-STAT1 and p-STAT3). In contrast, lower concentrations of ZnO NPs exerted no significant effect on LPS-induced STAT phosphorylation.

Given that STAT transcription factors are activated by JAK family members, we further examined JAK signaling activity. As depicted in Figure 6B, 5 μg/mL ZnO NPs treatment significantly inhibited LPS-induced phosphorylation of JAK1 (p-JAK1), whereas the phosphorylation level of JAK2 (p-JAK2) was unaffected. These findings demonstrate that ZnO NPs mitigate LPS-induced inflammatory responses by suppressing JAK1-mediated activation of STAT1 and STAT3.

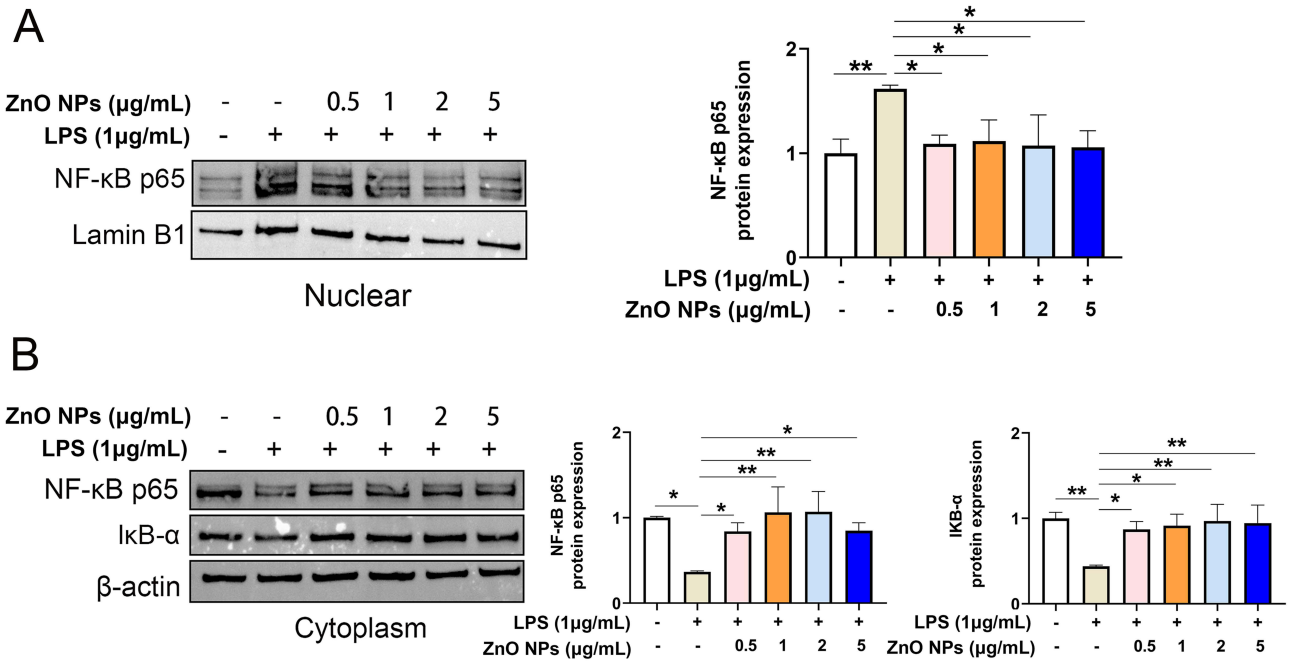

Figure 5 ZnO NPs inhibit the IκB-α/NF-κB pathway in RAW264.7 cells. RAW264.7 cells were pretreated with ZnO NPs (0–5 μg/mL) for 1 h prior to treatment with LPS (1 μg/mL) for 24 h. (**A** and **B**) Nuclear and cytoplasmic protein expressions of NF-κB p65 and IκB-α were detected by Western blot. Data are presented as mean ± SD and analyzed via one-way ANOVA. *p < 0.05 and **p < 0.01.

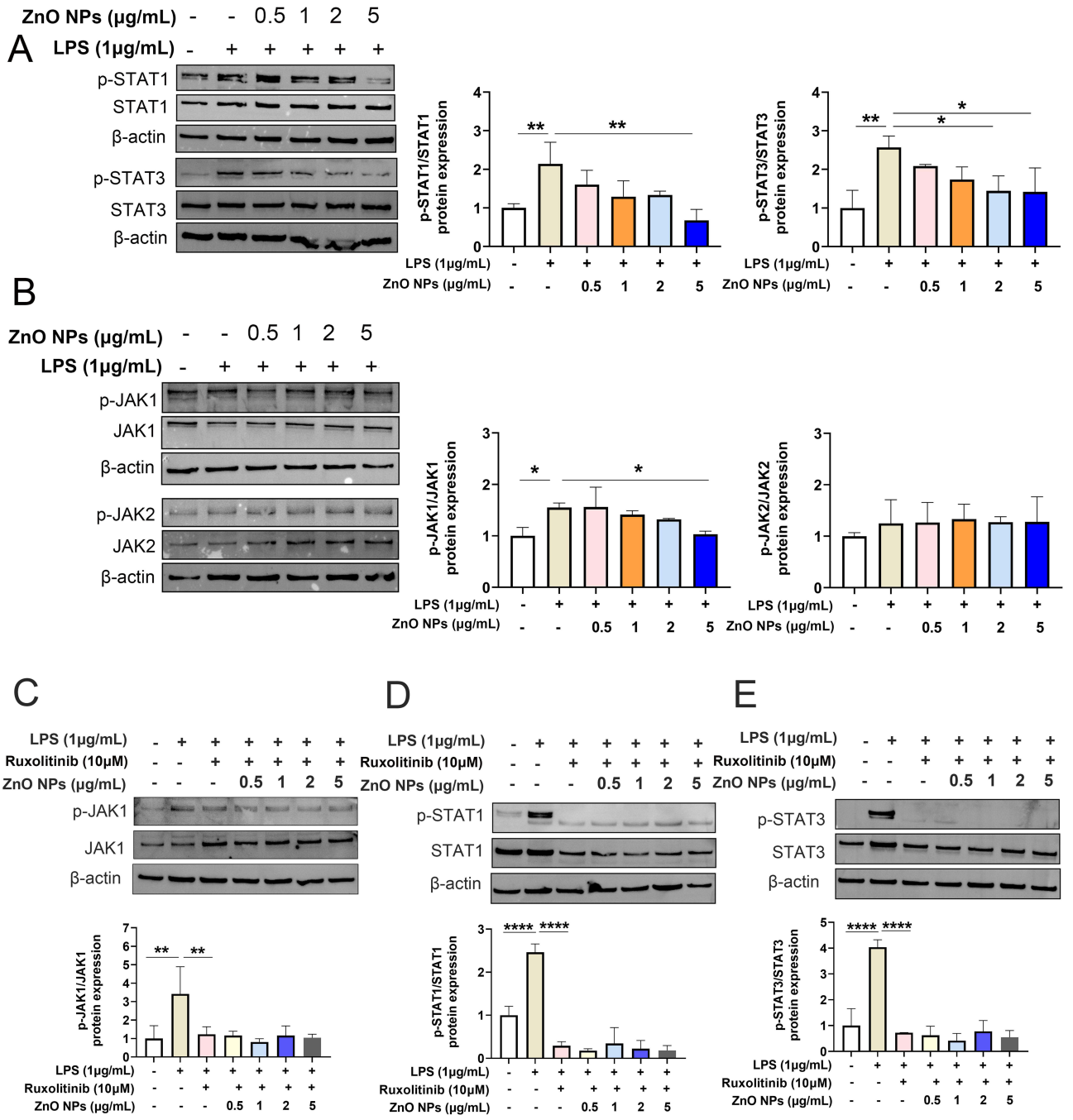

Figure 6 ZnO NPs suppress the JAK1-STAT1/STAT3 pathway in RAW264.7 cells. Cells were pretreated with ZnO NPs (0–5 μg/mL) for 1 h, followed by LPS (1 μg/mL) co-stimulation for 24 h. (**A**) The protein expressions of p-STAT1/STAT1, and p-STAT3/STAT3 were detected by Western blot. (**B**) The protein expressions of p-JAK1/ JAK1 and p-JAK2/ JAK2 were determined by Western blot. Separately, cells were pretreated with ZnO NPs (0–5 μg/mL) and 10 μM ruxolitinib for 1 h, followed by stimulation with LPS (1 μg/mL) for 24 h. (**C**–**E**) The protein levels of p-JAK1/ JAK1, p-STAT1/STAT1, and p-STAT3/STAT3 were determined by Western blot. Data are presented as mean ± SD and analyzed using one-way ANOVA. * $p < 0.05$, ** $p < 0.01$ and ****$p<0.0001$.

To further validate the anti-inflammatory effects of ZnO NPs mediated through inhibition of the JAK1-STAT1/STAT3 signaling pathways, we investigated whether the JAK-specific inhibitor ruxolitinib could mimic the anti-inflammatory effects of ZnO NPs. First, we determined the optimal concentration of ruxolitinib using a concentration gradient assay. The results showed that ruxolitinib at concentrations ≤10 μM exerted no cytotoxicity on RAW264.7 cells (Supplementary Figure 3). Therefore, RAW264.7 cells were treated with 10 μM ruxolitinib for 24 h in subsequent experiments. Compared to the LPS group, ruxolitinib completely suppressed the phosphorylation of JAK1, STAT1, and STAT3 (Figure 6C–E). Taken together,

https://doi.org/10.2147/JIR.S534720

these results demonstrate that JAK1 acts as a critical target for regulating LPS-induced inflammatory signaling pathways in RAW264.7 macrophages.

Furthermore, consistent with the aforementioned KEGG pathway enrichment analysis, we further examined three other inflammation-related signaling pathways: the PI3K/Akt pathway, NOD-like receptor pathway, and MAPK pathways. However, ZnO NPs treatment did not affect LPS-induced phosphorylation of JNK1/2, ERK1/2, or p38 (Supplementary Figure 4A–C). ZnO NPs also did not alter the phosphorylation level of PI3K, and neither LPS stimulation nor ZnO NPs affected the protein expression of p-Akt (Supplementary Figure 5A and B). Unexpectedly, neither LPS treatment nor ZnO NPs at different concentrations affected the protein expression of NOD1 or NOD2 (Supplementary Figure 6A and B). These findings indicate that ZnO NPs do not regulate the LPS-induced the PI3K/Akt pathway, MAPK pathway, or NOD-like receptor signaling pathway.

ZnO NPs Suppress LPS-Induced Nucleocytoplasmic Translocation of STAT1 and STAT3 in RAW264.7 Macrophages

Upon activation, STAT proteins undergo dimerization and translocate into the nucleus to initiate the transcription of target genes. To determine whether ZnO NPs inhibit the LPS-induced nuclear translocation of STAT1 and STAT3, we examined the subcellular localization of STAT1 and STAT3 in RAW264.7 cells following LPS stimulation. The results

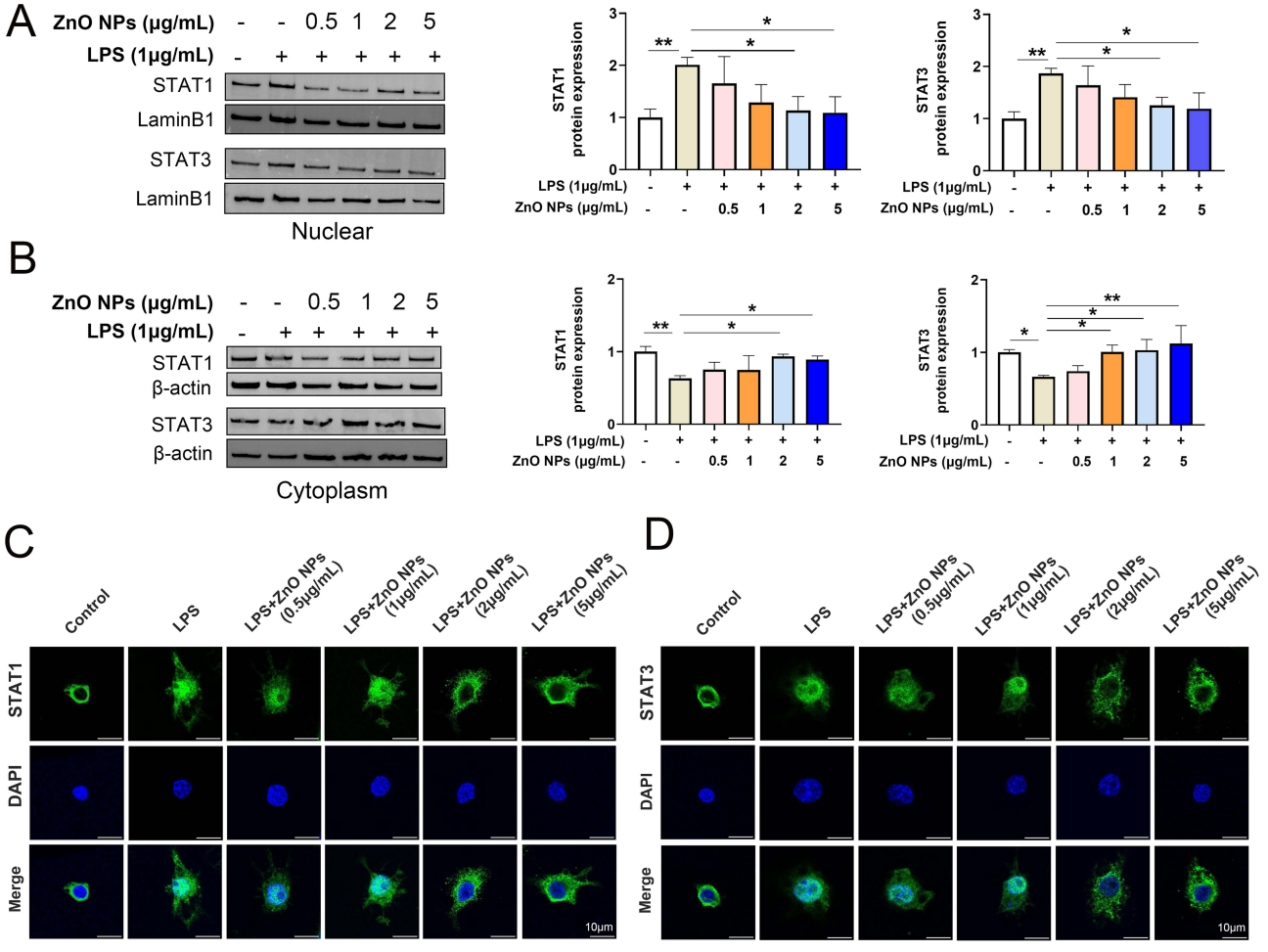

Figure 7 ZnO NPs suppress LPS-induced nuclear translocation of STAT1 and STAT3 in RAW264.7 cells. RAW264.7 cells were pretreated with ZnO NPs (0–5 μg/mL) for 1 h, followed by stimulation with LPS (1 μg/mL) for 24 h. (**A** and **B**) Nuclear and cytoplasmic protein expressions of STAT1 and STAT3 were analyzed by Western blot. (**C** and **D**) The subcellular localization of STAT1 and STAT3 were determined using confocal laser scanning microscopy (600× magnification). Data are presented as mean ±SD and analyzed by one-way ANOVA. *$p < 0.05$ and **$p < 0.01$.

showed that LPS treatment significantly induced the nuclear translocation of STAT1 and STAT3, whereas pretreatment with 2 and 5 μg/mL ZnO NPs markedly inhibited this LPS-induced translocation (Figure 7A and B).

We further examined the subcellular localization of STAT1 and STAT3 using confocal laser scanning microscopy. In the control group, STAT1 and STAT3 were primarily localized in the cytoplasm. In contrast, LPS treatment caused a marked translocation of STAT1 and STAT3 into the nucleus (Figure 7C and D). However, 2 and 5 μg/mL ZnO NPs significantly reduced this LPS-induced nucleocytoplasmic translocation of STAT1 and STAT3. These results were consistent with those from our WB analysis. Taken together, these findings demonstrate that ZnO NPs alleviate LPS-induced inflammatory responses by inhibiting JAK1-mediated activation of STAT1 and STAT3 and preventing their nuclear translocation.

ZnO NPs Mitigate LPS-Induced ROS Production in RAW264.7 Macrophages

As is well established, ROS contribute to the progression of inflammatory responses. To investigate whether the anti-inflammatory effects of ZnO NPs are linked to their capacity to suppress ROS accumulation, we evaluated LPS-induced ROS production in RAW264.7 cells. The results showed that ZnO NPs at lower concentrations (0.5–2 μg/mL) effectively inhibited LPS-induced ROS production; in contrast, ZnO NPs at 5 μg/mL failed to reduce such LPS-triggered ROS generation (Figure 8A–G). These findings demonstrate that ZnO NPs exhibit concentration-dependent antioxidant activity in RAW264.7 cells.

Discussion

Inflammatory diseases and related immune disorders are linked to high prevalence and mortality rates globally.[40] Thus, maintaining a balanced immune system is crucial for preventing inflammation-related diseases. In recent years, several studies have shown that ZnO NPs possesses anti-inflammatory properties.[32,35,41] Therefore, this study examines the effects of ZnO NPs on LPS-stimulated inflammation responses and explores the underlying molecular pathways in RAW264.7 cells.

First, SEM was employed to characterize the primary particle size of zinc ZnO NPs. Quantitative analysis of 400 randomly selected ZnO NPs revealed an average diameter of 180.7 ± 84.77 nm. Cell viability was subsequently assessed to evaluate potential cytotoxicity. Results showed that ZnO NPs at a concentration of 5 μg/mL did not significantly affect the viability of RAW264.7 cells. To further validate the in vitro biocompatibility of 5 μg/mL ZnO NPs, we conducted additional assays to assess changes in mitochondrial membrane potential and lysosomal membrane integrity. These experiments revealed no detectable disruption to either mitochondrial membrane potential or lysosomal structure in RAW264.7 cells treated with 5 μg/mL ZnO NPs, thus ruling out sub-lethal organelle damage. Therefore, we selected ZnO NP concentrations of 0.5, 1, 2, and 5 μg/mL for all subsequent in vitro experiments.

RAW264.7 macrophages are well-characterized for their secretion of diverse inflammatory mediators and pro-inflammatory cytokines, making them a robust model for studying inflammatory processes. NO, a key mediator of the oxidative stress response, plays a crucial role in the pathogenesis of inflammation-related diseases.[42] In the present study, we found that ZnO NPs at concentrations of 2 and 5 μg/mL significantly inhibited LPS-induced NO production. Beyond NO regulation, ZnO NPs suppressed LPS-induced production of the pro-inflammatory cytokines TNF-α, IL-1β, and IL-6 in various concentrations at both the transcriptional and protein levels. These findings align with previous reports: Meng et al reported that ZnO NPs mitigate the cytokines of TNF-α, IL-1β, and IL-6, induced by polymer wear particles.[32]

iNOS is an enzyme responsible for NO production, its expression precisely regulates intracellular NO levels, and serves as a critical molecular marker for evaluating inflammatory responses.[43] Additionally, COX-2 exhibits functional crosstalk with iNOS: prior studies have shown that NO or its metabolites can trigger the activation of COX enzymes, forming a regulatory loop that amplifies inflammatory responses.[44] Thus, targeting the expression of iNOS and COX-2 is a validated strategy for modulating inflammation. In this study, we found that ZnO NPs significantly inhibited LPS-induced mRNA and protein expression of iNOS and COX-2. However, a dose-dependent discrepancy was observed between transcriptional and protein expression levels: notably, M1 marker iNOS expression was significantly suppressed only at 5 μg/mL ZnO NPs, whereas COX-2 expression was effectively inhibited at both 2 and 5 μg/mL. Conversely, treatment with 5 μg/mL ZnO NPs significantly increased the expression of the M2 marker Arg-1. As is well established, M1 macrophages are contribute to pro-inflammatory responses, while M2 macrophages play a pivotal role in anti-

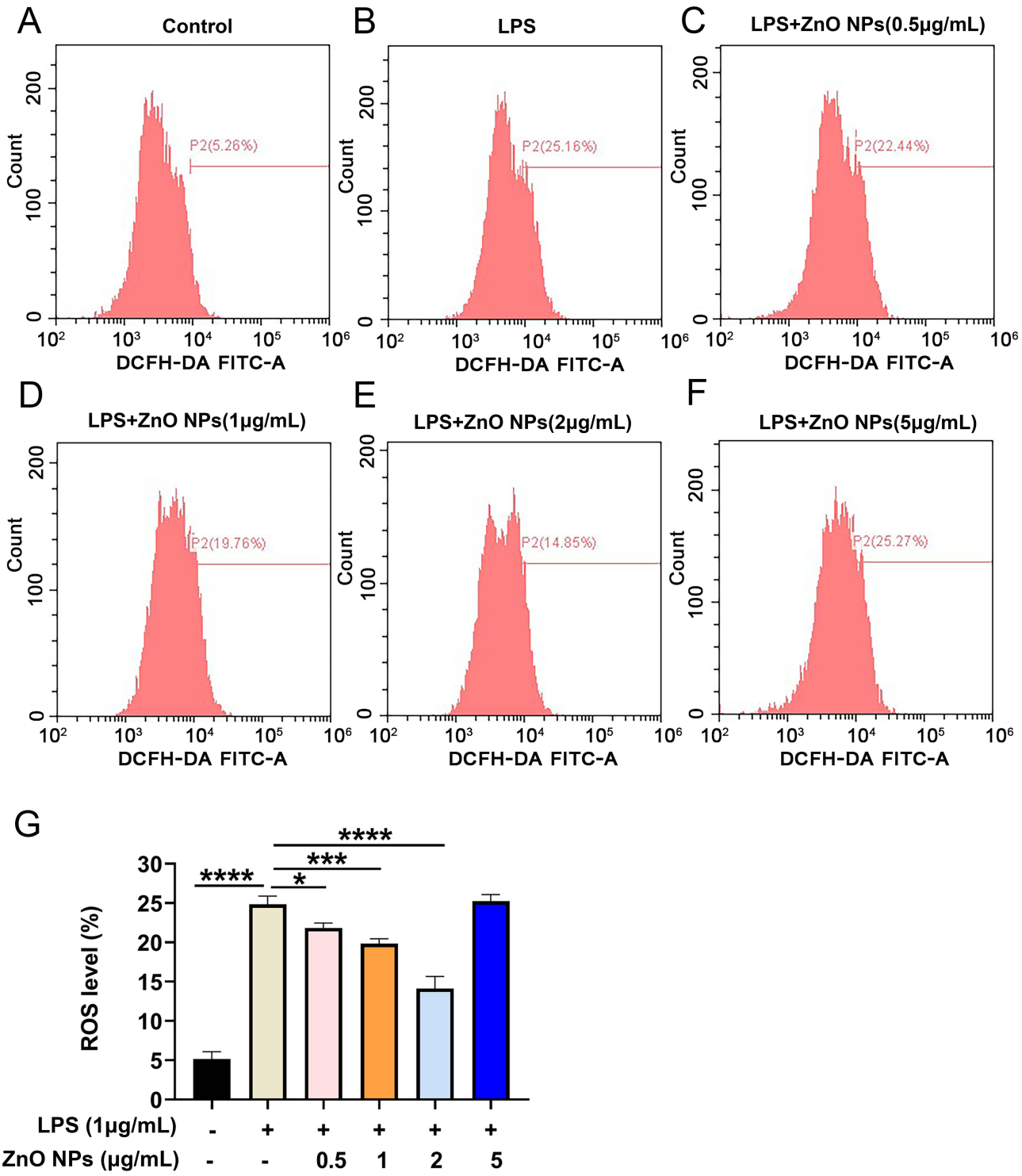

Figure 8 ZnO NPs inhibit intracellular ROS generation in RAW264.7 cells. RAW264.7 cells were pre-treated with ZnO NPs (0–5 μg/mL) for 1 h, followed by stimulation with LPS (1 μg/mL) for 24 h. (**A**–**F**) ROS fluorescence intensity was measured by flow cytometry. (**G**) Statistical analysis of ROS levels in different groups. Data are presented as mean ± SD and analyzed via one-way ANOVA. *p<0.05, ***p<0.001 and ****p<0.0001.

inflammatory processes and tissue repair.[45] Together, these data demonstrate that ZnO NPs not only inhibit the production of inflammatory mediators (NO) and pro-inflammatory cytokines but also modulate macrophage polarization by suppressing the M1 phenotype and promoting the M2 phenotype—with higher concentrations (5 μg/mL) exhibiting

more pronounced regulatory effects. This multimodal anti-inflammatory mechanism highlights the potential of ZnO NPs as a promising agent for mitigating LPS-induced inflammatory responses.

Furthermore, to gain deeper insights into the regulatory mechanisms by which ZnO NPs modulate macrophage-mediated inflammation, we performed, for the first time, RNA-seq analysis on RAW264.7 cells pretreated with ZnO NPs prior to LPS stimulation. A total of 3118 DEGs were identified in the LPS vs control comparison, whereas 2638 DEGs were detected in the LPS + ZnO NPs vs LPS comparison. KEGG pathway enrichment analysis revealed that multiple inflammation-related signaling pathways—including the TNF-α signaling pathway, NF-κB signaling pathway, JAK-STAT signaling pathway, NOD-like receptor signaling pathway, PI3K/Akt signaling pathway, and MAPK signaling pathway—play crucial roles in mediating the regulatory effects of ZnO NPs in the LPS-induced inflammation model. Notably, prior to our study, these pathways had not been systematically investigated in the context of ZnO NPs-regulated LPS-induced inflammation in RAW264.7 macrophages, which highlights the novelty of our findings. Consistent with existing literature, numerous studies have demonstrated that the JAK-STAT, MAPK, and NF-κB pathways play critical roles in LPS-induced inflammatory responses in macrophage.[46–48] However, there have been relatively few studies specifically investigating the pathway-specific regulatory effects of ZnO NPs on the aforementioned pathways. To address this research gap, we therefore carried out targeted mechanistic investigations into these pathways, aiming to clarify which of these key inflammatory signaling pathways—activated in LPS-stimulated RAW264.7 cells—can be modulated by ZnO NPs.

In general, NF-κB is retained in the cytoplasm by its inhibitor, IκBα. Upon LPS stimulation, upstream kinases—including IKKβ—phosphorylate IκBα, leading to its ubiquitin-proteasomal degradation. This degradation releases NF-κB p65, facilitating its translocation into the nucleus, where it modulates the expression of various inflammatory chemokines and cytokines.[49,50] In this study, we found that ZnO NPs at various concentrations—with the lowest being 0.5 μg/mL—all significantly suppressed LPS-induced IκBα degradation and inhibited the nuclear translocation of NF-κB p65. These findings demonstrate that ZnO NPs attenuate IκBα/NF-κB pathway activation by inhibiting p65 nuclear translocation, thereby subsequently reducing the expression of inflammatory cytokines.

The JAK-STAT pathway is recognized as a critical signaling cascade that regulates immune responses and inflammation.[51] Upon LPS binding to its receptors, receptor-associated JAK is activated. Once activated, STATs form dimers and translocate into the nucleus, where they bind to specific promoter sequences and transactivate the transcription of several target genes, such as iNOS.[52] In this study, we found that ZnO NPs at 5 μg/mL mitigate LPS-induced proinflammatory factor release by not only blocking JAK1-STAT1/3 activation but also preventing their (STAT1/STAT3) nuclear translocation. Ruxolitinib, a selective Janus kinase (JAK1/JAK2) inhibitor, has garnered significant attention for its role in modulating macrophage polarization, which is crucial in various inflammatory and immune responses.[53] Qi et al reported that 10 μM ruxolitinib, completely mimicked the anti-inflammatory effect of myricitrin, including inhibition of inflammatory cytokine expression and STAT1 activation.[54] Yang et al demonstrated that ruxolitinib inhibits fibrotic macrophage polarization by suppressing the JAK1/2-STAT6 signaling pathway, thereby alleviating bleomycin-induced lung fibrosis.[53] In order to explore whether ruxolitinib could mimic the anti-inflammatory effect of ZnO NPs, we performed rescue experiments. We found that compared to the LPS group, ruxolitinib could completely suppressed the phosphorylation of JAK1-STAT1/STAT3 signaling pathways. Taken together, our results demonstrate that JAK1 serves as a key target for regulating LPS-induced inflammatory signaling pathways in RAW264.7 macrophages.

The MAPK pathway also exerts a pivotal role in inflammatory processes. Canonical members of the MAPK family include extracellular signal-regulated kinases 1/2 (ERK1/2), c-Jun N-terminal kinases (JNK), and p38 mitogen-activated protein kinase (p38 MAPK).[55] Typically, LPS stimulation induces phosphorylation of ERK1/2, JNK, and p38, which in turn promotes nuclear translocation of the transcription factor AP-1 and upregulates the expression of pro-inflammatory mediators.[55] Notably, STAT transcription factors, activated by JAKs, exhibit crosstalk with ERKs and p38 MAPK in responses to porins[56] or LPS,[57] respectively. Additionally, vitro studies have indicated that serine/threonine phosphorylation of STAT1 and STAT3 is mediated by MAPKs.[58] Accordingly, we further investigated the impact of ZnO NPs on MAPK cascades. Unexpectedly, ZnO NPs pretreatment failed to modulate the phosphorylation of these MAPK family members, suggesting that ZnO NPs inhibit LPS-induced STAT1 and STAT3 phosphorylation independently of the MAPK pathway.

The PI3K/Akt signaling pathway has been shown to play a fundamental role in the initiation of inflammatory responses,[59] while it is also reported to participate in anti-inflammatory regulation. Notably, Yang et al reported that ablation of myeloid PTEN can activate PI3K/Akt signaling pathway, thereby mitigating the inflammatory response in acute liver injury.[60] Liu et al further demonstrated that myeloid PTEN deficiency can concomitantly activate phosphorylated Akt and inhibit phosphorylated GSK3β, which in turn suppresses inflammation in acute lung injury.[61] Additionally, Guo et al specifically reported that Sophoraflavanone G inhibits LPS-induced inflammation in RAW264.7 cells by targeting the PI3K/Akt signaling pathway.[62] However, in the present study, we found that ZnO NPs failed to inhibit LPS-induced phosphorylation of PI3K/Akt. Furthermore, NOD1 is one of the most prominent intracellular NOD-like receptors, acting as a crucial sensor of the innate immune system and is responsible for detecting diverse pathogens and stress signals arising from tissue injury.[63,64] Activation of NOD1 facilitates macrophage migration and enhances immune and inflammatory responses,[65] whereas disruption of NOD1 reduces inflammation in tissue injury.[66] Qu et al reported that macrophage Dvl2 deficiency promotes NOD1-driven pyroptosis and exacerbates inflammation during liver injury.[67] We further investigated the NOD1 and NOD2 signaling pathways; however, the results indicate that neither LPS nor ZnO NPs exert an effect on the protein expression of NOD1 and NOD2. In summary, these findings collectively indicate that ZnO NPs exert no effect on the PI3K/Akt and NOD1/NOD2 signaling pathways—even though both pathways are well-documented to be involved in inflammatory responses. In contrast, this study

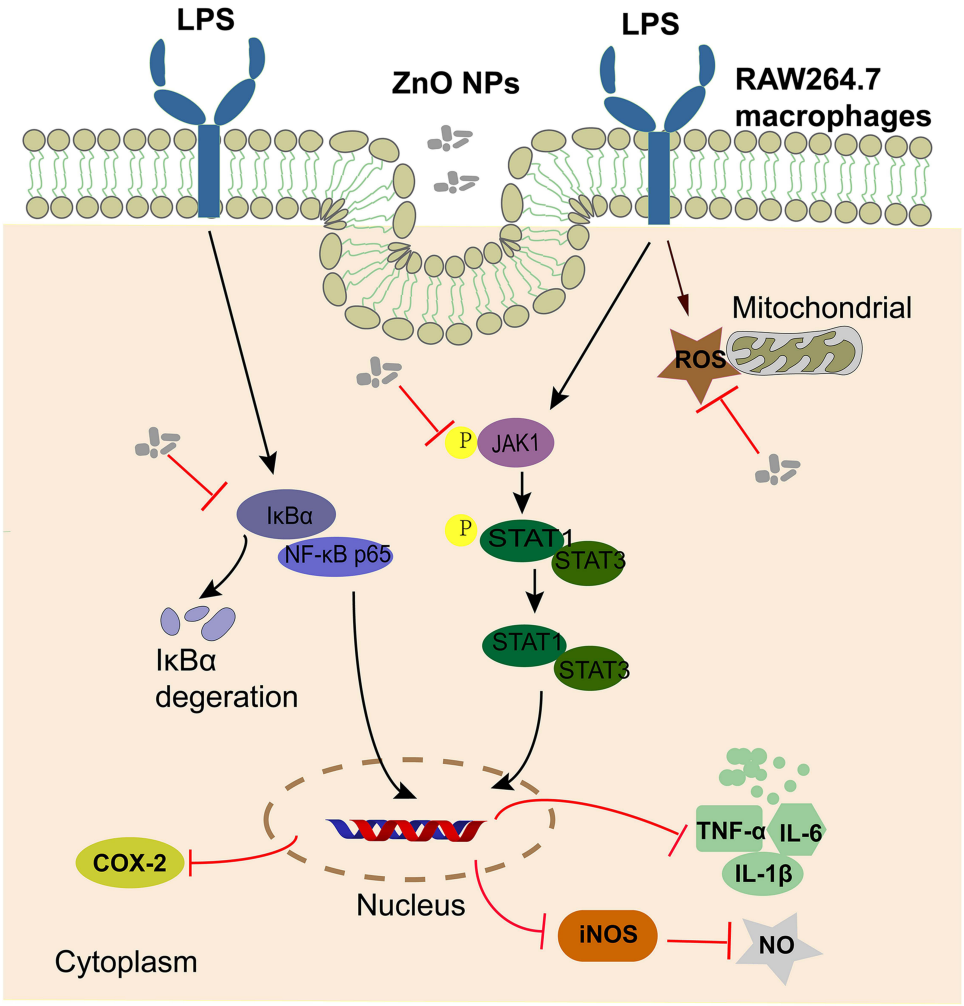

Figure 9 Schematic illustrating the anti-inflammatory mechanism of ZnO NPs in LPS-stimulated RAW264.7 cells. ZnO NPs exert anti-inflammatory effects by inhibiting the NF-κB and JAK1-STAT1/3 pathways and intracellular ROS generation; this in turn reduces the expression of pro-inflammatory mediators (iNOS and COX-2) and the production of NO, the release of pro-inflammatory cytokines (TNF-α, IL-1β and IL-6).

demonstrates that ZnO NPs can effectively inhibit LPS-induced inflammation by targeting the NF-κB and JAK1-STAT1 /STAT3 signaling pathways.

ROS function as secondary messengers, regulating the expression of pro-inflammatory gene.[68] While ROS function as signaling molecules in host defense responses, an excessive accumulation of ROS during inflammatory processes can lead to oxidative stress.[69,70] Oxidative stress, in turn, can activate various transcription factors, thereby driving the expression of genes involved in inflammatory pathways. Furthermore, Simon et al reported that ROS production contributes to the activation of the JAK-STAT pathway.[71] Consistent with this, Qi et al reported that inhibiting ROS generation can suppress JAK-STAT activation in RAW264.7 cells.[72] Moreover, ROS can intensify inflammatory responses through the activation of the NF-κB.[73] In the present study, we observed that lower concentrations of ZnO NPs (eg, 0.5, 1, and 2 μg/mL) reduced LPS-induced ROS generation in RAW264.7 cells. In contrast, 5 μg/mL ZnO NPs failed to inhibit LPS-induced ROS production. As established in our previous experiments, we have already ruled out the possibility that cytotoxicity contributed to this issue. Li et al reported that ulinastatin suppressed LPS-induced ROS production by activating the PI3K/Akt pathways.[74] Specifically, their study demonstrated that activated PI3K/Akt signaling can inhibit intracellular ROS generation—a key mechanistic link between this pathway and ROS regulation in LPS-stimulated models. In this study, we found that 5 μg/mL ZnO NPs failed to activate the PI3K/Akt pathway. This finding may partially explain why 5 μg/mL ZnO NPs cannot inhibit the LPS-indued the ROS production: at least, in part, due to their lack of PI3K/Akt activation. However, other specific regulatory mechanisms underlying this concentration-dependent behavior of ZnO NPs still remain to be further elucidated.

One major limitation of the present study lies in the absence of in vivo validation—while our in vitro data clearly and rigorously demonstrate the anti-inflammatory mechanisms of ZnO NPs in RAW264.7 macrophages, future studies should validate these anti-inflammatory effects and their underlying mechanisms in relevant animal models of macrophage-associated inflammatory disorders (eg, atherosclerosis models), thereby providing stronger evidence to support the therapeutic potential of ZnO NPs.

Conclusions

Collectively, our study demonstrates that ZnO NPs exert their anti-inflammatory effects by inhibiting the activation of the NF-κB and JAK1-STAT1/STAT3 signaling pathways, as well as by reducing intracellular ROS accumulation, in LPS-stimulated RAW264.7 cells (Figure 9). These findings provide novel insights into the molecular mechanisms underlying the anti-inflammatory properties of ZnO NPs and lay a foundation for their potential therapeutic applications in macrophage-associated inflammatory disorders.

Abbreviations

LPS, lipopolysaccharide; ZnO NPs, zinc oxide nanoparticles; NO, nitric oxide; ROS, reactive oxygen species; TNF-α, tumor necrosis factor-alpha; IL-1β, interleukin-1β; IL-6, interleukin-6; COX-2, cyclooxygenase 2; iNOS, inducible nitric oxide synthase; Arg-1, Arginase-1; NF-κB, Nuclear factor-κB; MAPK, mitogen-activated protein kinase; JAK-STAT, Janus kinase-signal transducer and activator of transcription; ERK1/2, extracellular signal-regulated kinases1/2; JNK, c-Jun N-terminal kinase; SEM, scanning electron microscopy; BP, biological processes; CC, cellular components; MF, molecular functions; PI3K/Akt, phosphatidylinositol 3-kinase-protein kinase B; NOD1, nucleotide-binding oligomerization domain 1; NOD2, nucleotide-binding oligomerization domain 2; qRT-PCR, Quantitative Real-time Polymerase Chain Reaction; GO, Gene Ontology; KEGG, Kyoto Encyclopedia of Genes and Genomes; GAPDH, housekeeping gene glyceraldehyde-3-phosphate dehydrogenase.

Data Sharing Statement

Any data involved in this study can be requested from the corresponding author.

Acknowledgments

This work was supported by the National Natural Science Foundation of China (Grant No. 82270535).

Disclosure

The authors declare that they have no competing interests in this work.

References

1. Alur I. Low-grade inflammation: a familiar factor in cardiovascular diseases. *JACC Basic Transl Sci*. 2023;8(11):1475. doi:10.1016/j.jacbts.2023.09.010
2. Chaudhary R, Prasad A, Agarwal V, et al. Chronic stress predisposes to the aggravation of inflammation in autoimmune diseases with focus on rheumatoid arthritis and psoriasis. *Int Immunopharmacol*. 2023;125(Pt A):111046. doi:10.1016/j.intimp.2023.111046
3. Holub M, Pottecher J, Herwald H, et al. Editorial: systemic inflammation in severe infectious diseases. *Front Immunol*. 2024;15:1483682. doi:10.3389/fimmu.2024.1483682
4. Pahwa R, Goyal A, Jialal I. *Chronic Inflammation*. StatPearls. Treasure Island (FL) ineligible companies; 2025.
5. Alshuweishi Y, Abudawood A, Alfayez D, et al. Platelet/High-density lipoprotein ratio (PHR) predicts type 2 diabetes in obese patients: a retrospective study. *Healthcare*. 2024;12(15):1540. doi:10.3390/healthcare12151540
6. Bosevski M, Stojanovska L, Apostolopoulos V. Inflammatory biomarkers: impact for diabetes and diabetic vascular disease. *Acta Biochim Biophys Sin*. 2015;47(12):1029–1031. doi:10.1093/abbs/gmv109
7. Ephraim R, Fraser S, Devereaux J, et al. Differential gene expression of checkpoint markers and cancer markers in mouse models of spontaneous chronic colitis. *Cancers*. 2023;15(19):4793. doi:10.3390/cancers15194793
8. Antoniades C, Chan K. Calcification vs inflammation: the modern toolkit for cardiovascular risk assessment. *JACC Cardiovasc Imaging*. 2024;17(10):1225–1228. doi:10.1016/j.jcmg.2024.08.006
9. Fernandez-Velasco M, Gonzalez-Ramos S, Bosca L. Involvement of monocytes/macrophages as key factors in the development and progression of cardiovascular diseases. *Biochem J*. 2014;458(2):187–193. doi:10.1042/BJ20131501
10. Bhattacharya M, Ramachandran P. Immunology of human fibrosis. *Nat Immunol*. 2023;24(9):1423–1433. doi:10.1038/s41590-023-01551-9
11. Frodermann V, Nahrendorf M. Macrophages and Cardiovascular Health. *Physiol Rev*. 2018;98(4):2523–2569. doi:10.1152/physrev.00068.2017
12. Frangogiannis NG. Cardiac fibrosis. *Cardiovasc Res*. 2021;117(6):1450–1488. doi:10.1093/cvr/cvaa324
13. Koenig AL, Shchukina I, Amrute J, et al. Single-cell transcriptomics reveals cell-type-specific diversification in human heart failure. *Nat Cardiovasc Res*. 2022;1(3):263–280. doi:10.1038/s44161-022-00028-6
14. Molenaar B, Timmer LT, Droog M, et al. Single-cell transcriptomics following ischemic injury identifies a role for B2M in cardiac repair. *Commun Biol*. 2021;4(1):146. doi:10.1038/s42003-020-01636-3
15. Na YR, Stakenborg M, Seok SH, et al. Macrophages in intestinal inflammation and resolution: a potential therapeutic target in IBD. *Nat Rev Gastroenterol Hepatol*. 2019;16(9):531–543. doi:10.1038/s41575-019-0172-4
16. Xu X, Yin P, Wan C, et al. Punicalagin inhibits inflammation in LPS-induced RAW264.7 macrophages via the suppression of TLR4-mediated MAPKs and NF-κB activation. *Inflammation*. 2014;37(3):956–965. doi:10.1007/s10753-014-9816-2
17. Shao J, Li Y, Wang Z, et al. 7b, a novel naphthalimide derivative, exhibited anti-inflammatory effects via targeted-inhibiting TAK1 following down-regulation of ERK1/2- and p38 MAPK-mediated activation of NF-κB in LPS-stimulated RAW264.7 macrophages. *Int Immunopharmacol*. 2013;17(2):216–228. doi:10.1016/j.intimp.2013.06.008
18. Azab A, Nassar A, Azab AN. Anti-inflammatory activity of natural products. *Molecules*. 2016;21(10):1321. doi:10.3390/molecules21101321
19. Sahoo SK, Parveen S, Panda JJ. The present and future of nanotechnology in human health care. *Nanomedicine*. 2007;3(1):20–31. doi:10.1016/j.nano.2006.11.008
20. Sanna V, Sechi M. Nanoparticle therapeutics for prostate cancer treatment. *Maturitas*. 2012;73(1):27–32. doi:10.1016/j.maturitas.2012.01.016
21. Lagopati N, Evangelou K, Falaras P, et al. Nanomedicine: photo-activated nanostructured titanium dioxide, as a promising anticancer agent. *Pharmacol Ther*. 2021;222:107795. doi:10.1016/j.pharmthera.2020.107795
22. Katifelis H, Nikou MP, Mukha I, et al. Ag/Au bimetallic nanoparticles trigger different cell death pathways and affect damage associated molecular pattern release in human cell lines. *Cancers*. 2022;14(6):1546. doi:10.3390/cancers14061546
23. Lagopati N, Kotsinas A, Veroutis D, et al. Biological effect of silver-modified nanostructured titanium dioxide in cancer. *Cancer Genomics Proteomics*. 2021;18(3 Suppl):425–439. doi:10.21873/cgp.20269
24. Vagena IA, Gatou MA, Theocharous G, et al. Functionalized ZnO-based nanocomposites for diverse biological applications: current trends and future perspectives. *Nanomaterials*. 2024;14(5):397. doi:10.3390/nano14050397
25. Behzad F, Sefidgar E, Samadi A, et al. An overview of zinc oxide nanoparticles produced by plant extracts for anti-tuberculosis treatments. *Curr Med Chem*. 2022;29(1):86–98. doi:10.2174/0929867328666210614122109
26. Mandal AK, Katuwal S, Tettey F, et al. Current research on zinc oxide nanoparticles: synthesis, characterization, and biomedical applications. *Nanomaterials*. 2022;12(17):3066. doi:10.3390/nano12173066
27. Rambabu K, Bharath G, Banat F, et al. Green synthesis of zinc oxide nanoparticles using Phoenix dactylifera waste as bioreductant for effective dye degradation and antibacterial performance in wastewater treatment. *J Hazard Mater*. 2021;402:123560. doi:10.1016/j.jhazmat.2020.123560
28. Hong H, Shi J, Yang Y, et al. Cancer-targeted optical imaging with fluorescent zinc oxide nanowires. *Nano Lett*. 2011;11(9):3744–3750. doi:10.1021/nl201782m
29. Prasanna APS, Venkataprasanna KS, Pannerselvam B, et al. Multifunctional ZnO/SiO(2) Core/Shell nanoparticles for bioimaging and drug delivery application. *J Fluoresc*. 2020;30(5):1075–1083. doi:10.1007/s10895-020-02578-z
30. Khorasani MT, Joorabloo A, Adeli H, et al. Design and optimization of process parameters of polyvinyl (alcohol)/chitosan/nano zinc oxide hydrogels as wound healing materials. *Carbohydr Polym*. 2019;207:542–554. doi:10.1016/j.carbpol.2018.12.021
31. Gatou MA, Lagopati N, Vagena IA, et al. ZnO nanoparticles from different precursors and their photocatalytic potential for biomedical use. *Nanomaterials*. 2022;13(1):122. doi:10.3390/nano13010122
32. Meng X, Zhang W, Lyu Z, et al. ZnO nanoparticles attenuate polymer-wear-particle induced inflammatory osteolysis by regulating the MEK-ERK-COX-2 axis. *J Orthop Translat*. 2022;34:1–10. doi:10.1016/j.jot.2022.04.001

33. Nagajyothi PC, Cha SJ, Yang IJ, et al. Antioxidant and anti-inflammatory activities of zinc oxide nanoparticles synthesized using Polygala tenuifolia root extract. *J Photochem Photobiol B*. 2015;146:10–17. doi:10.1016/j.jphotobiol.2015.02.008
34. Liu J, Kang Y, Yin S, et al. Key role of microtubule and its acetylation in a zinc oxide nanoparticle-mediated lysosome-autophagy system. *Small*. 2019;15(25):e1901073. doi:10.1002/smll.201901073
35. Mirza EH, Pan-Pan C, Wan Ibrahim WM, et al. Chondroprotective effect of zinc oxide nanoparticles in conjunction with hypoxia on bovine cartilage-matrix synthesis. *J Biomed Mater Res A*. 2015;103(11):3554–3563. doi:10.1002/jbm.a.35495
36. Ye Y, Xu Y, Lai Y, et al. Long non-coding RNA cox-2 prevents immune evasion and metastasis of hepatocellular carcinoma by altering M1/M2 macrophage polarization. *J Cell Biochem*. 2018;119(3):2951–2963. doi:10.1002/jcb.26509
37. Wang Y, Han B, Wang Y, et al. Mesenchymal stem cell-secreted extracellular vesicles carrying TGF-beta1 up-regulate miR-132 and promote mouse M2 macrophage polarization. *J Cell Mol Med*. 2020;24(21):12750–12764. doi:10.1111/jcmm.15860
38. Yu G, Wang LG, Han Y, et al. clusterProfiler: an R package for comparing biological themes among gene clusters. *OMICS*. 2012;16(5):284–287. doi:10.1089/omi.2011.0118
39. Kou X, Qi S, Dai W, et al. Arctigenin inhibits lipopolysaccharide-induced iNOS expression in RAW264.7 cells through suppressing JAK-STAT signal pathway. *Int Immunopharmacol*. 2011;11(8):1095–1102. doi:10.1016/j.intimp.2011.03.005
40. Furman D, Campisi J, Verdin E, et al. Chronic inflammation in the etiology of disease across the life span. *Nat Med*. 2019;25(12):1822–1832. doi:10.1038/s41591-019-0675-0
41. Zhang Y, Ding J, Wang Y, et al. Guanxinkang decoction attenuates the inflammation in atherosclerosis by regulating efferocytosis and MAPKs signaling pathway in LDLR(-/-) Mice and RAW264.7 cells. *Front Pharmacol*. 2021;12:731769. doi:10.3389/fphar.2021.731769
42. Xue LL, Wu WS, Ma X, et al. Modulation of LPS-induced inflammation in RAW264.7 murine cells by novel isoflavonoids from Millettia pulchra. *Bioorg Chem*. 2020;97:103693. doi:10.1016/j.bioorg.2020.103693
43. Lawrence T, Willoughby DA, Gilroy DW. Anti-inflammatory lipid mediators and insights into the resolution of inflammation. *Nat Rev Immunol*. 2002;2(10):787–795. doi:10.1038/nri915
44. Swierkosz TA, Mitchell JA, Warner TD, et al. Co-induction of nitric oxide synthase and cyclo-oxygenase: interactions between nitric oxide and prostanoids. *Br J Pharmacol*. 1995;114(7):1335–1342. doi:10.1111/j.1476-5381.1995.tb13353.x
45. Shapouri-Moghaddam A, Mohammadian S, Vazini H, et al. Macrophage plasticity, polarization, and function in health and disease. *J Cell Physiol*. 2018;233(9):6425–6440. doi:10.1002/jcp.26429
46. Lee SB, Lee WS, Shin JS, et al. Xanthotoxin suppresses LPS-induced expression of iNOS, COX-2, TNF-alpha, and IL-6 via AP-1, NF-κB, and JAK-STAT inactivation in RAW 264.7 macrophages. *Int Immunopharmacol*. 2017;49:21–29. doi:10.1016/j.intimp.2017.05.021
47. Zhou Y, Wang J, Yang W, et al. Bergapten prevents lipopolysaccharide-induced inflammation in RAW264.7 cells through suppressing JAK/STAT activation and ROS production and increases the survival rate of mice after LPS challenge. *Int Immunopharmacol*. 2017;48:159–168. doi:10.1016/j.intimp.2017.04.026
48. Han BH, Lee YJ, Yoon JJ, et al. Hwangryunhaedoktang exerts anti-inflammation on LPS-induced NO production by suppressing MAPK and NF-κB activation in RAW264.7 macrophages. *J Integr Med*. 2017;15(4):326–336. doi:10.1016/S2095-4964(17)60350-9
49. Ishii M, Nakahara T, Araho D, et al. Glycolipids from spinach suppress LPS-induced vascular inflammation through eNOS and NK-κB signaling. *Biomed Pharmacother*. 2017;91:111–120. doi:10.1016/j.biopha.2017.04.052
50. Xu R, Ma L, Chen T, et al. Sophorolipid suppresses LPS-induced inflammation in RAW264.7 cells through the NF-κB signaling pathway. *Molecules*. 2022;27(15). doi:10.3390/molecules27155037
51. Shuai K, Liu B. Regulation of JAK-STAT signalling in the immune system. *Nat Rev Immunol*. 2003;3(11):900–911. doi:10.1038/nri1226
52. Levy DE, Darnell JE. Stats: transcriptional control and biological impact. *Nat Rev Mol Cell Biol*. 2002;3(9):651–662. doi:10.1038/nrm909
53. Yang Z, Li Z, Liu Z, et al. Ruxolitinib attenuates bleomycin-induced pulmonary fibrosis in mice by modulating macrophage polarization through the JAK/STAT signaling pathway. *Int Immunopharmacol*. 2025;161:114962. doi:10.1016/j.intimp.2025.114962
54. Qi S, Feng Z, Li Q, et al. Myricitrin modulates NADPH oxidase-dependent ROS production to inhibit endotoxin-mediated inflammation by blocking the JAK/STAT1 and NOX2/p47 phox pathways. *Oxid Med Cell Longev*. 2017;2017(1):9738745. doi:10.1155/2017/9738745
55. Chang L, Karin M. Mammalian MAP kinase signalling cascades. *Nature*. 2001;410(6824):37–40. doi:10.1038/35065000
56. Hwang KY, Oh YT, Yoon H, et al. Baicalein suppresses hypoxia-induced HIF-1alpha protein accumulation and activation through inhibition of reactive oxygen species and PI 3-kinase/Akt pathway in BV2 murine microglial cells. *Neurosci Lett*. 2008;444(3):264–269. doi:10.1016/j.neulet.2008.08.057
57. Kisseleva T, Bhattacharya S, Braunstein J, et al. Signaling through the JAK/STAT pathway, recent advances and future challenges. *Gene*. 2002;285(1–2):1–24. doi:10.1016/s0378-1119(02)00398-0
58. Galdiero M, Vitiello M, D'Isanto M, et al. STAT1 and STAT3 phosphorylation by porins are independent of JAKs but are dependent on MAPK pathway and plays a role in U937 cells production of interleukin-6. *Cytokine*. 2006;36(5–6):218–228. doi:10.1016/j.cyto.2006.12.003
59. He L, Pan Y, Yu J, et al. Decursin alleviates the aggravation of osteoarthritis via inhibiting PI3K-Akt and NF-kB signal pathway. *Int Immunopharmacol*. 2021;97:107657. doi:10.1016/j.intimp.2021.107657
60. Yang T, Qu X, Zhao J, et al. Macrophage PTEN controls STING-induced inflammation and necroptosis through NICD/NRF2 signaling in APAP-induced liver injury. *Cell Commun Signal*. 2023;21(1):160. doi:10.1186/s12964-023-01175-4
61. Liu Y, Zhou W, Zhao J, et al. Regulation of YAP translocation by myeloid Pten deficiency alleviates acute lung injury via inhibition of oxidative stress and inflammation. *Free Radic Biol Med*. 2024;222:199–210. doi:10.1016/j.freeradbiomed.2024.06.016
62. Guo C, Yang L, Luo J, et al. Sophoraflavanone G from Sophora alopecuroides inhibits lipopolysaccharide-induced inflammation in RAW264.7 cells by targeting PI3K/Akt, JAK/STAT and Nrf2/HO-1 pathways. *Int Immunopharmacol*. 2016;38:349–356. doi:10.1016/j.intimp.2016.06.021
63. Keestra-Gounder AM, Byndloss MX, Seyffert N, et al. NOD1 and NOD2 signalling links ER stress with inflammation. *Nature*. 2016;532(7599):394–397. doi:10.1038/nature17631
64. Travassos LH, Carneiro LA, Girardin SE, et al. Nod1 participates in the innate immune response to Pseudomonas aeruginosa. *J Biol Chem*. 2005;280(44):36714–36718. doi:10.1074/jbc.M501649200
65. Motomura Y, Kanno S, Asano K, et al. Identification of pathogenic cardiac CD11c+ macrophages in Nod1-mediated acute coronary arteritis. *Arterioscler Thromb Vasc Biol*. 2015;35(6):1423–1433. doi:10.1161/ATVBAHA.114.304846

66. Gonzalez-Ramos S, Fernandez-Garcia V, Recalde M, et al. Deletion or inhibition of NOD1 favors plaque stability and attenuates atherothrombosis in advanced atherogenesis (dagger). *Cells*. 2020;9(9). doi:10.3390/cells9092067
67. Qu X, Xu D, Yang T, et al. Macrophage Dvl2 deficiency promotes NOD1-Driven pyroptosis and exacerbates inflammatory liver injury. *Redox Biol*. 2025;79:103455. doi:10.1016/j.redox.2024.103455
68. Pan JS, Hong MZ, Ren JL. Reactive oxygen species: a double-edged sword in oncogenesis. *World J Gastroenterol*. 2009;15(14):1702–1707. doi:10.3748/wjg.15.1702
69. Park HS, Kim SR, Lee YC. Impact of oxidative stress on lung diseases. *Respirology*. 2009;14(1):27–38. doi:10.1111/j.1440-1843.2008.01447.x
70. Li Q, Verma IM. NF-κB regulation in the immune system. *Nat Rev Immunol*. 2002;2(10):725–734. doi:10.1038/nri910
71. Simon AR, Rai U, Fanburg BL, et al. Activation of the JAK-STAT pathway by reactive oxygen species. *Am J Physiol*. 1998;275(6):C1640–1652. doi:10.1152/ajpcell.1998.275.6.C1640
72. Qi Z, Yin F, Lu L, et al. Baicalein reduces lipopolysaccharide-induced inflammation via suppressing JAK/STATs activation and ROS production. *Inflamm Res*. 2013;62(9):845–855. doi:10.1007/s00011-013-0639-7
73. El-Shitany NA, Eid B. Proanthocyanidin protects against cisplatin-induced oxidative liver damage through inhibition of inflammation and NF-kappabeta/TLR-4 pathway. *Environ Toxicol*. 2017;32(7):1952–1963. doi:10.1002/tox.22418
74. Li ST, Dai Q, Zhang SX, et al. Ulinastatin attenuates LPS-induced inflammation in mouse macrophage RAW264.7 cells by inhibiting the JNK/NF-κB signaling pathway and activating the PI3K/Akt/Nrf2 pathway. *Acta Pharmacol Sin*. 2018;39(8):1294–1304. doi:10.1038/aps.2017.143